Design of safety-oriented control allocation strategies for overactuated electric vehicles

Ricardo de Castro[a], Mara Tanelli[b*], Rui Esteves Araújo[c] and Sergio M. Savaresi[b]

[a]Institute of System Dynamics and Control, Robotics and Mechatronics Center, German Aerospace Center (DLR), Wessling D-82234, Germany; [b]Dipartimento di Elettronica, Informazione e Bioingegneria, Politecnico di Milano, Piazza Leonardo da Vinci 32, 20133 Milano, Italy; [c]Faculdade de Engenharia da Universidade do Porto, Rua Dr. Roberto Frias, s/n 4200-465 Porto, Portugal

(*Received 1 November 2013; accepted 13 April 2014*)

1. Introduction and motivation

Torque allocation for over-actuated electric vehicles (EVs) is a very interesting and challenging research topic in automotive systems. Such modern vehicle architectures, in fact, offer a plurality of actuators that allow the designer to actively shape and adapt the vehicle dynamic response. This can be performed by properly setting up hierarchical control problems that regulate the vehicle motion by allocating the forces/torques at the wheels and solving constrained control allocation problems tailored to jointly optimise different cost functions that can be either safety, or energy, or performance-oriented (or, most interestingly, combinations of all these aspects).[1] Usually, the high-level motion objectives are expressed in terms of imposing a desired yaw moment to the vehicle, which must then be transformed into wheel torque reference signals. When the actuators are installed in the same axle, e.g. with torque vectoring devices or with two in-wheel motors (IWMs), the allocation is easy

*Corresponding author. Email:
tanelli@elet.polimi.it

to perform because there is a one-to-one mapping between the yaw moment and the torque difference.[2–4] On the other hand, if four IWMs (4IWMs) are present there is redundancy in the moment generation, which can be explored to minimise the energy consumption [1,5] or other performance metrics. As a matter of fact, 4IWMs and four-wheel steer (4WS) EV platforms represent the key enabling technology for the optimal management of the vehicle motion and of its energy flows, as it allows a significant freedom in the generation of the actual control commands, that can be selected in view of competing requirements. To start with, note that this redundant actuation structure allows us to actively regulate the longitudinal and lateral forces that each wheel produces.[6] This property paves the way for using the centre of gravity (CoG) forces and moments as the pseudo-control variables, which in turn introduces major simplifications to the motion controller's design.[6,7] In addition, the high degree of manoeuvrability introduced by the 4WS also facilitates the generation of feasible paths for the vehicle, e.g. with this structure it is possible to impose zero side-slip motions or perform parallel manoeuvres.[8]

Given the high degree of actuation redundancy present in the considered class of vehicles, there are many allocation solutions that are able to fulfil the force and yaw-moment demands determined by the high-level motion control system. In this work, the actuation redundancy is explored by a control allocation technique that intends to enhance safety by minimising the tyre friction use, while considering the actuation limits. To solve this problem, two techniques are investigated. The first extends the cascading generalised inverse (CGI) technique,[9,10] a well-known technique borrowed from aeronautical applications, to the force allocation problem in a vehicular context. More specifically, it is shown that, by fixing *a priori* the direction of the force at each tyre (obtained from the pseudo-inverse solution of the unconstrained optimisation problem), the allocation problem can be transformed into a practical quadratic-programming (QP) problem. Simulation results demonstrate that, as long as the requested forces are feasible, this approach is capable of generating accurate solutions in less than 400 μs (average values). However, for unfeasible force requests, the performance of this allocation strategy significantly degrades. This issue led us to develop a second approach, based on the linearisation of the tyre–road friction constraints. Albeit requiring a computational time that is 2–3 times higher than the previous strategy, the linearisation-based approach induces reduced allocation errors with respect to the extended CGI technique, particularly for unfeasible force requests.

The contributions of this work are thus twofold:

- the high-level motion controller contains feedback (FB) mechanisms, based on generalised speed loops, which are derived within a sliding mode framework and are endowed with conditional integrators.[11,12] Besides its implementation and tuning simplicity, robustness to disturbances and built-in anti-wind-up mechanisms, the conditional integrators also offer a chattering-alleviated operation, thus mitigating one of the main issues in traditional sliding control laws. Further, the stability properties of the closed loop are formally assessed.
- at the lower control layer, the motion controller needs to determine the wheel torques and steer angles that are needed to apply the (CoG) forces and moments requested by the motion controller to the vehicle. To do this, the two aforementioned force allocation strategies are proposed and compared.

The effectiveness of the proposed controller is demonstrated with simulation tests, carried out with the help of the full-vehicle CarSim simulator.

With respect to the conference paper,[13] this work presents extensions in several directions: first of all a closed-loop formulation of the motion control problem in terms of a

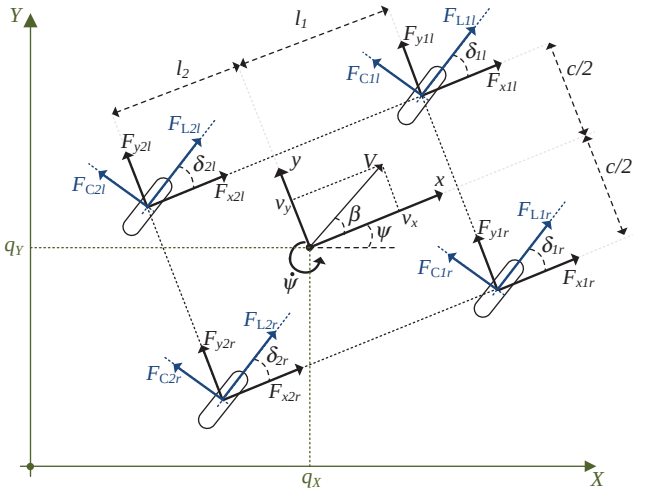

Figure 1. Two-track vehicle model.

speed reference tracking is provided, and its stability properties analysed. Then, a new safety-oriented objective is pursued (rather than the performance-only approach based on minimum-time manoeuvre followed in [13]), and the related force allocation step is detailed in two different algorithms that explore the computational complexity and the allocation error issues. Further, a full-vehicle simulation environment is considered to assess the performance of the approach in a more realistic setting.

The structure of the paper is as follows. Section 2 introduces the vehicle dynamics of interest, while Section 3 introduces the proposed controller architecture and defines the control problem. Section 4 presents the motion controller, formally analysing the closed-loop stability. Further, Section 5 addresses the force allocation problem, illustrating the two proposed approaches. Finally, Section 6 illustrates the results of the tests performed with the CarSim simulator.

2. Vehicle model

The vehicle under study is composed of four independent wheel drive commanded by the four IWMs and four independent wheel steering. To make the mathematical model tractable, the roll and pitch dynamics of the EV will be neglected, which is a typical assumption in the development of control-oriented models for the vehicle dynamics.[2,7,14]

In what follows, front and rear tyres will be indicated with the subscript 1 and 2, left and right with l and r. They will be compactly grouped in the set $\mathfrak{T} = \{1l, 1r, 2l, 2r\}$.

2.1. *Preliminaries*

Consider the vehicle represented in Figure 1 of mass m and yaw inertia I_z. The velocity of the CoG in the xy frame (integral to the car) is given by

$$\mathbf{v} = [v_x \;\; v_y \;\; \dot{\psi}]^{\mathrm{T}}, \tag{1}$$

where v_x is the vehicle longitudinal speed, v_y the lateral speed and $\dot{\psi}$ the yaw rate. The generalised forces/moments ($\mathcal{F}$) applied to the CoG are represented as

$$\mathcal{F} = [F_x \;\; F_y \;\; M_z]^{\mathrm{T}}, \tag{2}$$

where F_x and F_y are the longitudinal and lateral forces applied to the CoG, and M_z is the yaw moment. This global force is the aggregated result of the individual friction forces generated by each tyre and is given by

$$\mathcal{F} = \mathbf{B}\mathbf{F}_{xy}, \quad \mathbf{B} = \begin{bmatrix} B_x \\ B_y \\ B_\psi \end{bmatrix} = \begin{bmatrix} 1 & 0 & 1 & 0 & 1 & 0 & 1 & 0 \\ 0 & 1 & 0 & 1 & 0 & 1 & 0 & 1 \\ -\frac{c}{2} & l_1 & \frac{c}{2} & l_1 & -\frac{c}{2} & -l_2 & \frac{c}{2} & -l_2 \end{bmatrix},$$

where l_1 and l_2 are the distances between front and rear axle and the CoG, c the track width and $\mathbf{F}_{xy}$ are the tyre friction in the xy frame (Figure 1), namely

$$\mathbf{F}_{xy} = [F_{x1l} \;\; F_{y1l} \;\; F_{x1r} \;\; F_{y1r} \;\; F_{x2l} \;\; F_{y2l} \;\; F_{x2r} \;\; F_{y2r}]^{\mathrm{T}}.$$

Finally, the frictional forces generated by each tyre are usually modelled in the local coordinates LC, fixed with the wheel (see again Figure 1). The variables in the LC coordinates are related to those in the xy frame as

$$\begin{bmatrix} F_{xi} \\ F_{yi} \end{bmatrix} = \underbrace{\begin{bmatrix} \cos(\delta_i) & -\sin(\delta_i) \\ \sin(\delta_i) & \cos(\delta_i) \end{bmatrix}}_{\mathbf{W}(\delta_i)} \begin{bmatrix} F_{\mathrm{L}i} \\ F_{\mathrm{C}i} \end{bmatrix}, \quad i \in \mathfrak{T}, \tag{3}$$

where $F_{\mathrm{L}i}$ is the force generated along the tyre axis, $F_{\mathrm{C}i}$ the cornering force (orthogonal to the tyre axis) and δ_i is the steering angle of the ith wheel. Note that the inverse $\mathbf{W}^{-1}(\delta_i)$ is well defined for all values of δ_i.

2.2. *Equation of motion*

By direct application of Newton's law, the dynamic evolution of the vehicle velocity $\mathbf{v}$ is

$$\mathbf{M} \underbrace{\begin{bmatrix} -v_y\dot{\psi} \\ v_x\dot{\psi} \\ 0 \end{bmatrix}}_{g(\mathbf{v})} + \mathbf{M}\dot{\mathbf{v}} = \mathcal{F} - \mathcal{R}(\mathbf{v}) + \mathcal{D}, \tag{4}$$

where $\mathbf{M} = \mathrm{diag}([m, m, I_z])$, $\mathcal{D} \in \mathbb{R}^3$ a generalised bounded force due to the effect of non-modelled dynamics and disturbances and $\mathcal{R}(\mathbf{v}) \in \mathbb{R}^3$ represents the resistance forces opposing the vehicle motion (see Appendix 1) for its description.

2.3. *Friction forces*

As already mentioned, the generalised force/moments $\mathcal{F}$ are a direct consequence of the individual friction forces, $F_{\mathrm{L}i}, F_{\mathrm{C}i}$, generated by each tyre. To model these forces, a simplified version of the well-known Pacejka magic formula will be employed.[15] The main inputs for this model are (i) the longitudinal tyre slip κ_i, which is the normalised difference between the wheel rotational speed (ω_i) and the wheel linear speed ($v_{\mathrm{L}i}$); and (ii) the tyre side-slip angle

α_i, which is the angle between the wheel axis (δ_i) and its velocity vector. Formally, these variables are defined as

$$\kappa_i = \frac{\omega_i r_i - v_{\mathrm{L}i}}{v_{\mathrm{L}i}}, \quad \tan\alpha_i = -\frac{v_{\mathrm{C}i}}{v_{\mathrm{L}i}}, \quad i \in \mathfrak{T}, \tag{5}$$

where r_i is the effective radius of the wheel and $v_{\mathrm{L}i}$, $v_{\mathrm{C}i}$ are the tyre longitudinal and cornering speeds. Such speeds can be also written as [16]

$$\begin{bmatrix} v_{\mathrm{L}i} \\ v_{\mathrm{C}i} \end{bmatrix} = \mathbf{W}^{-1}(\delta_i) \begin{bmatrix} 1 & 0 & \chi_{\mathrm{L}i} \\ 0 & 1 & \chi_{\mathrm{C}i} \end{bmatrix} \mathbf{v}, \quad i \in \mathfrak{T}, \tag{6}$$

$$[\chi_{\mathrm{L}1l} \;\; \chi_{\mathrm{L}1r} \;\; \chi_{\mathrm{L}2l} \;\; \chi_{\mathrm{L}2r}] = \left[-\frac{c}{2} \;\; \frac{c}{2} \;\; -\frac{c}{2} \;\; \frac{c}{2}\right],$$

$$[\chi_{\mathrm{C}1l} \;\; \chi_{\mathrm{C}1r} \;\; \chi_{\mathrm{C}2l} \;\; \chi_{\mathrm{C}2r}] = [l_1 \;\; l_1 \;\; -l_2 \;\; -l_2].$$

To express the combined slip conditions, needed to model situations where traction and steering are simultaneously applied, the so-called *theoretical slips* [15] are considered:

$$\sigma_{\mathrm{L}i} = \frac{\kappa_i}{1+\kappa_i}, \quad \sigma_{\mathrm{C}i} = \frac{\tan\alpha_i}{1+\kappa_i}, \quad \sigma_i = \sqrt{{\sigma_{\mathrm{L}i}}^2 + {\sigma_{\mathrm{C}i}}^2}, \quad i \in \mathfrak{T}.$$

They are responsible for the longitudinal ($F_{\mathrm{L}i}$) and cornering forces ($F_{\mathrm{C}i}$) of the tyre, namely

$$\begin{aligned} F_{\mathrm{L}i} = \frac{\sigma_{\mathrm{L}i}}{\sigma_i} F_i(\sigma_i, F_{zi}), \quad F_{\mathrm{C}i} = \frac{\sigma_{\mathrm{C}i}}{\sigma_i} F_i(\sigma_i, F_{zi}) \\ F_i(\sigma_i, F_{zi}) = \mu_{\max} F_{zi} \sin\left(C\mathrm{atan}(B\sigma_i)\right), \quad i \in \mathfrak{T}, \end{aligned} \tag{7}$$

where C and B are parameters of the friction model, $\mu_{\max}$ is the tyre–road friction peak and F_{zi} the vertical force.

Remark 1 The longitudinal ($F_{\mathrm{L}i}$) and cornering ($F_{\mathrm{C}i}$) forces of the tyre must fulfil

$$F_{\mathrm{L}i}^2 + F_{\mathrm{C}i}^2 = F_i^2 \leq (\mu_{\max} F_{zi})^2, \quad i \in \mathfrak{T}. \tag{8}$$

This is known in the literature as the friction circle constraint. For simplicity, the above representation of the tyre–road friction forces assumes an isotropic distribution, which leads to the friction circle constraint.

Remark 2 The friction circle constraint also holds for the forces defined in the xy coordinates, which are confined to the following set:

$$F_{xi}^2 + F_{yi}^2 = \left\| \mathbf{W}(\delta_i) \begin{bmatrix} F_{\mathrm{L}i} \\ F_{\mathrm{C}i} \end{bmatrix} \right\|_2^2 = F_i^2 \leq (\mu_{\max} F_{zi})^2, \quad i \in \mathfrak{T}.$$

This property results from the fact that the change of coordinates $\mathbf{W}(\delta_i)$ does not affect the magnitude of the tyre force.

2.4. *Vertical forces*

The tyre vertical forces F_{zi} are affected by the load transfer between front–rear axle and left–right wheels, which the vehicle experiences when subject to longitudinal and lateral accelerations. To model these factors, a quasi-static mapping is used,[16]

$$\begin{aligned}
&\mathbf{F}_z = \mathbf{F}_z^0 + \varrho_x a_x + \varrho_y a_y,\\
&\mathbf{F}_z = [F_{z1l}\ \ F_{z1r}\ \ F_{z2l}\ \ F_{z2r}]^{\mathrm{T}}, \quad \mathbf{F}_z^0 = \frac{mg}{2(l_1+l_2)}[l_2\ \ l_2\ \ l_1\ \ l_1]^{\mathrm{T}},\\
&\varrho_x = \frac{mh}{2(l_1+l_2)}[-1\ \ -1\ \ 1\ \ 1]^{\mathrm{T}}, \quad \varrho_y = \frac{mh}{c(l_1+l_2)}[-l_2k_f\ \ l_2k_f\ \ -l_1k_r\ \ l_1k_r]^{\mathrm{T}},
\end{aligned} \tag{9}$$

where $\mathbf{F}_z^0$ is the static force distribution, h is the height of the CoG, k_f and k_r represent the front and rear coefficients associated with the lateral load transfer approximated based on roll stiffness distribution,[17] g is the gravitational acceleration and a_x and a_y the longitudinal and lateral accelerations, respectively

2.5. *Wheel dynamics and actuator limits*

The rotational dynamics of each wheel in the vehicle is given by

$$J\dot{\omega}_i = T_i - r_i F_{\mathrm{L}i}, \quad i \in \mathfrak{T},$$

where J is the wheel inertia and T_i the wheel torque. We assume that the wheel torque is generated by a combination of IWMs ($T_{\mathrm{m},i}$) and brake-by-wire actuators ($T_{\mathrm{b},i}$), i.e. $T_i = T_{\mathrm{m},i} + T_{\mathrm{b},i}$. The main limiting factors in these actuators are the acceleration power and acceleration torque limits associated with the IWMs, which yield

$$\underline{T} \le T_i \le \bar{T}, \quad T_i\omega_i \le \bar{P}, \quad i \in \mathfrak{T}, \tag{10}$$

where $\bar{T} \in \mathbb{R}_+$ is the maximum acceleration torque that the motor can develop, $\underline{T} \in \mathbb{R}_-$ the maximum braking torque of the brake-by-wire system and $\bar{P}$ the maximum acceleration power, which are equal for all wheels. The braking power limits are not explicitly considered here, since, due to safety issues, modern braking systems are generally able to overcome the friction limits. In other words, the constraints introduced by the friction circle (8) will be the dominant factor in the generation of the braking torque (and not the power limits of the braking system).

As for the steering, it is assumed that each wheel has independent steer capabilities, constrained to the following sets:

$$-\bar{\delta} \le \delta_i \le \bar{\delta}, \quad i \in \mathfrak{T}, \tag{11}$$

where $\bar{\delta}$ is the maximum steering range. The dynamics of all the actuators are neglected, since, in practice, in the considered vehicle platform their bandwidth is significantly higher than that of the vehicle dynamics of interest.

2.6. *Compact representation*

In summary, the vehicle model can be compactly represented as

$$\mathbf{M}\dot{\mathbf{v}} = -\mathbf{M}g(\mathbf{v}) + \mathcal{F} - \mathcal{R}(\mathbf{v}) + \mathcal{D}, \tag{12a}$$

$$\mathcal{F} = \mathbf{B}\mathbf{F}_{xy}, \tag{12b}$$

$$\mathbf{F}_{xy,i} = \mathbf{W}(\delta_i)[F_{\mathrm{L}i} \;\; F_{\mathrm{C}i}]^{\mathrm{T}}, \quad i \in \mathfrak{T}, \tag{12c}$$

$$\begin{bmatrix} F_{\mathrm{L}i} \\ F_{\mathrm{C}i} \end{bmatrix} = \tilde{\mathbf{F}}_i(\mathbf{v}, \omega_i, \delta_i, F_{zi}, \theta_T), \quad i \in \mathfrak{T}, \tag{12d}$$

$$\mathbf{F}_z = \mathbf{F}_z^0 + \frac{\varrho_x}{m}\mathbf{e}_1^{\mathrm{T}}(\mathcal{F} - \mathcal{R}) + \frac{\varrho_y}{m}\mathbf{e}_2^{\mathrm{T}}(\mathcal{F} - \mathcal{R}), \tag{12e}$$

$$J\dot{\omega}_i = T_i - r_i F_{\mathrm{L}i}, \quad i \in \mathfrak{T}, \tag{12f}$$

$$\underline{T} \leq T_i \leq \bar{T}, \quad T_i\omega_i \leq \bar{P}, \quad -\bar{\delta} \leq \delta_i \leq \bar{\delta}, \quad i \in \mathfrak{T}, \tag{12g}$$

where $\tilde{\mathbf{F}}_i \in \mathbb{R}^2$ is the friction force, which groups Equations (5)–(7), θ_T represents the parameters of the friction model, $\mathbf{F}_{xy,i}$ refers to the x and y force components of the tyre $i \in \mathfrak{T}$ and $\mathbf{e}_1^{\mathrm{T}} = [1 \;\; 0 \;\; 0]^{\mathrm{T}}$, $\mathbf{e}_2^{\mathrm{T}} = [0 \;\; 1 \;\; 0]^{\mathrm{T}}$.

From a control perspective, T_i and δ_i are the model inputs, and $\mathbf{v}$ the system states. Note that the motion controller will be designed under the assumption that the wheel torques T_i can be individually regulated. Given that T_i is a result of both the IWM ($T_{\mathrm{m},i}$) and the brake-by-wire system ($T_{\mathrm{b},i}$), it will be necessary to perform torque allocation among these actuators, particularly for $T_i < 0$. In this work, we will assume that the torque allocation is performed by the hybrid ABS algorithm presented by de Castro et al.[18]

3. Controller specification and architecture

The main goal of the motion controller is to determine the torque and steer values for each wheel, T_i, δ_i, so that the vehicle follows a given (generalised) speed reference, while fulfilling all existing constraints. As already mentioned, this work considers a by-wire powertrain configuration, where the torque and steering angles applied to the wheels are imposed through electric and electro-mechanical actuators. Since this configuration does not have a mechanical connection between the driver and the actuators, the use of advanced human–machine interfaces (HMIs) is necessary. The HMI block is normally responsible for (i) translating the driver inputs (e.g. displacements of the throttle pedal, braking pedal, steering and other inputs) into appropriate motion demands for the car, (ii) providing haptic FB to the driver and (iii) incorporating desired reference models for the vehicle transient behaviour. In what follows, we will assume that the HMI translates the driver requests into a (generalised) speed reference of the form

$$\mathbf{v}_r = [v_{x,r} \;\; v_{y,r} \;\; \dot{\psi}_r.]^{\mathrm{T}} \tag{13}$$

It will be further assumed that this (generalised) speed reference is feasible and its first-order time derivative $\dot{\mathbf{v}}_r$ is known.

In the light of the nonlinearities that affect the vehicle model, the design of a control law for T_i, δ_i that will make $\mathbf{v}$ follow $\mathbf{v}_r$ is not obvious nor trivial, mainly due to the friction force generation mechanisms, specified by Equations (12b)–(12d). To cope with this issue, a model inversion approach for the friction forces will be adopted. The idea is to design the controller under the assumption that the CoG forces and moments $\mathcal{F}$ can be individually

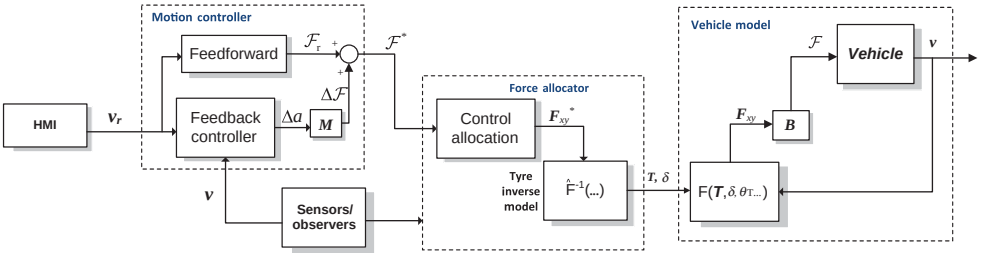

Figure 2. Block diagram of the proposed control algorithm.

regulated. Inspecting Equation (12), one can immediately conclude that using $\mathcal{F}$ as the virtual control input (instead of the true inputs T_i and δ_i) enables us to decouple the generation of the friction forces from the vehicle dynamics (**v**), bringing undeniable advantages for the design of the motion controller. Accordingly, the controller proposed in this work will track the vehicle speed **v** using $\mathcal{F}$ as the virtual control input (see block diagram in Figure 2). The generation of the true inputs T_i and δ_i will be then performed by the force allocation block. Another important aspect that deserves discussion is the availability of the FB signals. In this work, it is assumed that the state **v** and the wheels rotational speed ω_i are available for FB. While some of these signals are easily measured, such as $\dot{\psi}$ and ω_i, others require dedicated sensors and/or observers. Even if it is still not common to have all these signals available in everyday cars, the trend in the automotive industry is towards the increased availability of these signals,[7,19] which is made easier in the advanced vehicle platforms as the one considered herein.

4. Motion controller

The main goal for the motion controller design (Figure 2) can be formulated as follows: devise a law for $\mathcal{F}$ that will make the vehicle velocity **v** track the speed profile $\mathbf{v}_r$, in spite of the disturbance $\mathcal{D}$. In the ideal case ($\mathcal{D} \equiv 0$), the control task can be accomplished by simply using the feedforward (FF) term $\mathcal{F}_r$

$$\mathcal{F}_\mathbf{r} = \mathbf{M}(g(\mathbf{v}_r) + \dot{\mathbf{v}}_r) + \mathcal{R}(\mathbf{v}_r). \tag{14}$$

Since, in practice, there are both unmodelled dynamics and disturbances, these cause non-zero tracking errors $\mathbf{e}_v = \mathbf{v} - \mathbf{v}_r$, with the following dynamics:

$$\mathbf{M}\dot{\mathbf{e}}_v = \mathcal{F} - \mathcal{F}_r + \mathbf{M}(g(\mathbf{v}_r) - g(\mathbf{v})) + \mathcal{R}(\mathbf{v}_r) - \mathcal{R}(\mathbf{v}) + \mathcal{D}. \tag{15}$$

Based on the input–output linearisation technique,[20] the most relevant nonlinearities in the above model can be cancelled by selecting the CoG force as

$$\mathcal{F} = \underbrace{\mathbf{M}\Delta a}_{\Delta\mathcal{F}} + \mathcal{F}_r - \mathbf{M}(g(\mathbf{v}_r) - g(\mathbf{v})) - \mathcal{R}(\mathbf{v}_r) + \mathcal{R}(\mathbf{v}), \tag{16}$$

where $\Delta a \in \mathbb{R}^3$ represents acceleration increments (a new virtual control variable) that will be directly manipulated by the controller. This makes the error model be

$$\dot{\mathbf{e}}_v = \Delta a + \mathcal{D}_a, \tag{17}$$

where $\mathcal{D}_a = \mathbf{M}^{-1}\mathcal{D} \in \mathbb{R}^3$ are the equivalent accelerations due to $\mathcal{D}$. Note that, albeit Equation (16) assumes exact knowledge of some model parameters (e.g. **M**), in practice the influence

of these parametric errors can be effortlessly embedded in $\mathcal{D}_a$. To facilitate the design of the controller, it is convenient to represent the above multiple input, multiple output system as a set of three single input, single output ones:

$$\dot{e}_{vj} = \Delta a_j + \mathcal{D}_{aj}, \tag{18}$$

where $j \in \mathfrak{J} = \{x, y, \psi\}$ represents the subscript associated with each degree of freedom in the vehicle local coordinate system. The main challenge in the design of the speed tracking controller lies in the effective attenuation of $\mathcal{D}_{aj}$. To cope with this difficulty, we explore a sliding-mode formulation, endowed with conditional integrators.[11,12] The proposed control law is given by

$$\Delta a_j = -k_{aj}\text{sat}\left(\frac{\sigma_j}{\varepsilon_j}\right), \tag{19a}$$

$$\sigma_j = e_{vj} + k_{\eta j}\eta_j, \tag{19b}$$

$$\dot{\eta}_j = -k_{\eta j}\eta_j + \varepsilon_j \text{sat}\left(\frac{\sigma_j}{\varepsilon_j}\right), \quad j \in \mathfrak{J}, \tag{19c}$$

where k_{aj}, $k_{\eta j}$, ε_j are the controller parameters, η_j the gain of the (conditional) integrator, σ_j the sliding variable and $\text{sat}(w) = \text{sgn}(w)\min(1, |w|)$ the saturation function. The properties of the resulting closed-loop system can be stated as follows.

PROPOSITION 4.1 *Consider system* (18)*, controlled by Equation* (19)*. It holds that*

(1) *if* $|\eta_j(0)| \leq \varepsilon_j/k_{\eta j}$*, then* $|\eta_j(t)| \leq \varepsilon_j/k_{\eta j}$*, for* $t \geq 0$;
(2) *for an arbitrary bounded disturbance* $\mathcal{D}_{aj} \leq \bar{\mathcal{D}}_{aj}$*, and assuming*

$$k_{aj} > \bar{\mathcal{D}}_{aj} + 2k_{\eta j}\varepsilon_j, \quad j \in \mathfrak{J}, \tag{20}$$

then system state will reach in finite time the set

$$\Xi_j = \left\{|e_{vj}| \leq 2\varepsilon_j, \quad |\sigma_j| \leq \frac{\varepsilon_j}{k_{\eta j}}\right\} \subset \mathbb{R}^2, \quad j \in \mathfrak{J}; \tag{21}$$

(3) *moreover, if* (*i*) *the disturbance is Lipschitz in the domain* Ξ_j*, i.e.*

$$|\mathcal{D}_{aj}(e_a) - \mathcal{D}_{aj}(e_b)| \leq L_j|e_a - e_b| \quad \forall e_a, e_b \in \{|x| \leq 2\varepsilon_j\},$$

where L_j *is the Lipschitz constant,* $j \in \mathfrak{J}$*; and* (*ii*) *the controller parameters fulfil*

$$k_{\eta j} > 0, \quad 0 < \varepsilon_j < \frac{4k_{\eta j}k_{aj}}{4k_{\eta j}L_j + (L_j k_{\eta j} + 1)^2}; \tag{22}$$

then, the tracking error, besides reaching Ξ_j*, will asymptotically converge to zero, i.e.* $e_{vj} \to 0$.

Proof The proof is omitted for space limitations and can be found in [21]. ■

The above results show that, for (general) bounded disturbances, the absolute value of the tracking error e_{vj} will be ultimately bounded by $2\varepsilon_j$. Asymptotic convergence to zero can be ensured for the (particular) case where $\mathcal{D}_{aj}$ is locally Lipschitz. For controller tuning, let

us first consider the operation in the linear range. In particular, for $|\sigma_j| \leq \varepsilon_j$, the saturation functions in Equation (19) become linear, resulting in the following control law:

$$\Delta a_j = -\frac{k_{aj}}{\varepsilon_j} e_{vj} - \frac{k_{aj}}{\varepsilon_j} k_{\eta j} \eta_j, \tag{23}$$

$$\dot{\eta}_j = e_{vj}, \quad |e_{vj} + k_{\eta j} \eta_j| \leq \varepsilon_j. \tag{24}$$

Thus, the proposed controller operates as a simple proportional/integral controller when the sliding variable is small. In light of this interpretation, we can now appreciate the practical benefits of the first claim in Proposition 4.1: the bound $|\eta_j(t)| \leq \varepsilon_j / k_{\eta j}$ endows the controller with an anti-wind-up mechanism that deals with the saturation of the integral action. Moreover, when in a linear regime, the closed-loop dynamics can be expressed as

$$\begin{bmatrix} \dot{\eta}_j \\ \dot{e}_{vj} \end{bmatrix} = \begin{bmatrix} 0 & 1 \\ -\frac{k_{aj}}{\varepsilon_j} k_{\eta j} & -\frac{k_{aj}}{\varepsilon_j} \end{bmatrix} \begin{bmatrix} \eta_j \\ e_{vj} \end{bmatrix} + \begin{bmatrix} 0 \\ \mathcal{D}_{aj} \end{bmatrix}, \tag{25}$$

which yields the following second-order characteristic polynomial:

$$\lambda^2 + \underbrace{\frac{k_{aj}}{\varepsilon_j}}_{2\zeta_j \omega_{nj}} \lambda + \underbrace{\frac{k_{aj}}{\varepsilon_j} k_{\eta j}}_{\omega_{nj}^2} = 0, \quad j \in \mathfrak{J}, \tag{26}$$

where ω_{nj}, ζ_j are the natural frequency and damping, respectively, of the (undisturbed) closed-loop dynamics.

5. Force allocation strategies

This section is devoted to the force allocation problem, which constitutes the final step for the application of the motion control commands to the vehicle. First the ideal allocation problem is discussed, and then its practical implementation is addressed, with two different approaches that are proposed and compared.

5.1. *Ideal allocation problem*

Once the motion controller outputs the desired value of $\mathcal{F}^* = \mathcal{F}_r + \mathbf{M}\Delta a$, it is necessary to allocate the wheel torques T_i and steer angles δ_i capable of actually producing $\mathcal{F}^*$. In this work, the allocation is performed through the force allocation layer depicted in Figure 2. Given the high level of redundancy in the vehicle, the allocation solution is, in general, not unique, and this opens the door to pursue secondary goals, such as the minimisation of the energy consumption of the actuators and/or friction utilisation of tyres. In the literature, this type of problem is known as control allocation [22,23] and can be formulated as

$$\min_{T_i, \delta_i, \mathbf{F}_{xy}, F_{\mathrm{L}i}, F_{\mathrm{C}i}, \mathbf{F}_z, \omega_i} \quad L(\cdot) + \|\mathbf{Q}\mathbf{z}\|_p^p, \tag{27a}$$

$$\mathcal{F}^* = \mathbf{B}\mathbf{F}_{xy} + \mathbf{z}, \tag{27b}$$

$$\mathbf{F}_{xy,i} = \mathbf{W}(\delta_i)[F_{\mathrm{L}i} \;\; F_{\mathrm{C}i}]^{\mathrm{T}}, \quad i \in \mathfrak{T}, \tag{27c}$$

$$\begin{bmatrix} F_{\mathrm{L}i} \\ F_{\mathrm{C}i} \end{bmatrix} = \tilde{\mathbf{F}}_i(\mathbf{v}, \omega_i, \delta_i, F_{zi}, \theta_T), \quad i \in \mathfrak{T}, \tag{27d}$$

$$\mathbf{F}_z = \mathbf{F}_z^0 + \left(\frac{\varrho_x}{m}\mathbf{e}_1^{\mathrm{T}} + \frac{\varrho_y}{m}\mathbf{e}_2^{\mathrm{T}}\right)\mathbf{B}\mathbf{F}_{xy}, \tag{27e}$$

$$\mathbf{F}_z > 0, \tag{27f}$$

$$T_i = r_i F_{\mathrm{L}i}, \quad i \in \mathfrak{T}, \tag{27g}$$

$$\underline{T} \leq T_i \leq \bar{T}, \quad T_i\omega_i \leq \bar{P}, \quad -\bar{\delta} \leq \delta_i \leq \bar{\delta}, \quad i \in \mathfrak{T}. \tag{27h}$$

The function $L(\cdot)$ is a performance metric associated with the secondary goals of the allocation (to be defined shortly), $\mathbf{z} \in \mathbb{R}^3$ is a slack variable that allows tolerating non-feasible requests for $\mathcal{F}^*$, $p \in \{1, 2\}$ is the type of norm employed and $\mathbf{Q} = \mathrm{diag}([Q_x \;\; Q_y \;\; Q_z]) \in \mathbb{R}^{3\times 3}$ is a diagonal matrix which assigns individual penalisations to the allocation errors. The problem constraints are related to the friction force mechanism and the limitations of the actuators introduced in Section 2. It must be pointed out that (i) the vehicle speed $\mathbf{v}$ is considered as known, (ii) the vertical forces $\mathbf{F}_z$ are constrained to positive values (in order to avoid wheel lift) and (iii) steady-state conditions for the wheel rotational dynamics are assumed. This means that the torque and the longitudinal tyre force are related by the static map (27g), while the wheel rotational ω_i is used as an additional optimisation variable (that affects directly the wheel longitudinal slip and the friction force).

5.2. *Practical allocation approaches*

Due to the nonlinearities in Equation (27), obtaining a numerical solution for this problem is in general difficult, particularly for real-time applications. In the control allocation literature dedicated to automotive applications, two main approaches are used to overcome this issue. The first idea is to linearise the friction model around the current operating point. For instance, by joining all the friction-related constraints of Equation (27), one may find a compact nonlinear map between $\mathcal{F}^*$, the vehicle speed ($\mathbf{v}$) and the control inputs $\mathbf{u} = [T_i, \delta_i, \ldots]$, that is, $\mathcal{F}^* = \mathbf{f}(\mathbf{v}, \mathbf{u})$. Linearising the model around $(\mathbf{v}^{\mathrm{eq}}, \mathbf{u}^{\mathrm{eq}})$ gives

$$\mathcal{F}^* \approx \mathbf{f}(\mathbf{v}^{\mathrm{eq}}, \mathbf{u}^{\mathrm{eq}}) + \left.\frac{\partial \mathbf{f}(\mathbf{v}, \mathbf{u})}{\partial \mathbf{u}}\right|_{\mathbf{v}^{\mathrm{eq}}, \mathbf{u}^{\mathrm{eq}}} \Delta\mathbf{u}. \tag{28}$$

Thus, the original nonlinear friction is replaced by an affine relation, and the increment $\Delta\mathbf{u}$ can be used as the new control input; the final control value is then obtained as $\mathbf{u} = \mathbf{u}^{\mathrm{eq}} + \Delta\mathbf{u}$, where $\mathbf{u}^{\mathrm{eq}}$ is the nominal operation point of the controller (obtained, for example, in the previous control iteration) and $\mathbf{v}^{\mathrm{eq}}$ is the current vehicle speed. With this approach, the nonlinear constraints are relaxed to linear relations, which call for simple linear or QP solvers (assuming that the cost function is linear or quadratic, respectively), as discussed in [7,24,25].

The second possibility for solving Equation (27) builds on the idea of exerting a direct control over the *xy* forces of the tyres, i.e. $\mathbf{F}_{xy}$ is considered as a second virtual control. This approach is very attractive for vehicles with independent wheel steer and independent wheel drive as those considered herein, since, in principle, each tyre can generate force in an arbitrary direction. Additionally, the use of $\mathbf{F}_{xy}$ as a virtual control enables us to decompose the allocation problem in two steps, the first of which determines the *xy* force distribution among the tyres in order to fulfil the force/moment requested to the CoG, yielding

$$\min_{\mathbf{z}, \mathbf{F}_{xy}, \mathbf{F}_z} \quad L(\cdot) + \|\mathbf{Q}\mathbf{z}\|_p^p, \tag{29a}$$

$$\mathcal{F}^* = \mathbf{B}\mathbf{F}_{xy} + \mathbf{z}, \tag{29b}$$

$$\|\mathbf{E}_i\mathbf{F}_{xy}\|_2 \leq \mu_{\max} F_{zi}, \quad i \in \mathfrak{T}, \tag{29c}$$

$$\mathbf{F}_z = \mathbf{F}_z^0 + \left(\frac{\varrho_x}{m}\mathbf{e}_1^{\mathrm{T}} + \frac{\varrho_y}{m}\mathbf{e}_2^{\mathrm{T}}\right)\mathbf{B}\mathbf{F}_{xy}, \tag{29d}$$

$$\mathbf{F}_z > 0, \tag{29e}$$

$$[1 \;\; 0]\mathbf{E}_i\mathbf{F}_{xy} \leq \min\left(\frac{\bar{T}}{r_i}, \frac{\bar{P}}{v_x}\right) \quad \forall i \in \mathfrak{T}. \tag{29f}$$

For this approximation, the torque and power limits of the motors are approximated using the considerations discussed in Appendix 3, while the friction limits are treated as described in [21]. Note that the above constraints are convex: Equation (29c) can be posed as a second-order cone, while the remaining one is linear. Thus, if the performance metric $L(\cdot)$ is convex, the resulting optimisation problem is also convex,[26] which brings undeniable theoretical advantages in comparison to the original formulation (27) (e.g. any local solution is also global). After solving the above problem, the second step in the allocation process relies on the inversion of the tyre forces. Namely, using the $\mathbf{F}_{xy}$ obtained from Equation (29) and the vehicle state $\mathbf{v}$, one must find the torque (T_i) and steer (δ_i) that yield the desired tyre forces. As shown in [21], for the slip-based friction model under consideration here, such inversion is possible and the involved computations are manageable. Different versions of this approach have been reported in the literature.[6,27–29]

In comparison with the linearisation approach, the main advantage of using $\mathbf{F}_{xy}$ as a second virtual control is that of maintaining the nonlinearities in the friction model. On the other hand, the formulation (29) makes it more difficult to translate the physical actuator limits (torque and steer) to the *xy* force components, which generally calls for the approximation of the actuator constraints (as explained in Appendix 3). Interestingly, the introduction of the physical actuator limits is not an issue for the linearisation approach and can easily be incorporated in the allocation problem. In summary, the designer has two practical routes to formulate the force allocation problem: (i) linearise the friction model and use the true physical limits of the actuators [7,24,25]; or (ii) employ the full nonlinear friction model and approximate the physical actuator limits.[6,27–29] In this work, we will follow the second approach and concentrate our attention on the application of fast numerical techniques to handle the control allocation problem, which can be used in real-time applications. This is motivated by the fact that we intend to choose, as secondary performance metric, the minimisation of the tyre friction force for safety maximisation. Thus, it is important to employ the most accurate description of the forces available.

5.3. *Performance metric and control allocation problem*

Due to overactuation in the vehicle, there are many possibilities to allocate the forces among the tyres. To exploit this redundancy, we will consider, as a secondary performance metric, the minimisation of the friction used in the tyre, i.e.

$$\begin{aligned} L(\mathbf{F}_{xy}, \mathbf{F}_z) &= \sum_{i\in\mathfrak{T}} \left\| \frac{1}{\mu_{\max} F_{zi}} \mathbf{E}_i \mathbf{F}_{xy} \right\|^2 = \sum_{i\in\mathfrak{T}} \left\| \begin{bmatrix} \frac{1}{\mu_{\max} F_{zi}} & 0 \\ 0 & \frac{1}{\mu_{\max} F_{zi}} \end{bmatrix} \begin{bmatrix} F_{xi} \\ F_{yi} \end{bmatrix} \right\|^2 \\ &= \|\mathbf{R}^*(\mathbf{F}_z)\mathbf{F}_{xy}\|^2, \end{aligned} \tag{30}$$

where $\mathbf{R}^*(\mathbf{F}_z)$ is a diagonal matrix, which assigns the weight $1/\mu_{\max}F_{zi}$ to the x and y forces of the ith tyre.

The idea behind the performance metric L is to assign to each tyre a penalisation that is inversely proportional to the vertical force that each wheel supports. Consequently, the tyres with higher vertical forces, thus capable of delivering larger forces, will have lower penalisation, while the lighter tyres will be forced to produce less force. Since this allocation policy discourages the full use of friction forces, it can also be viewed, to some extent, as maximisation of a safety margin in the force allocation. In order to facilitate the practical use of this cost function, it will be further assumed that the allocation errors, $\mathbf{z}$, are not too large, which enables us to approximate the weight matrix as

$$\begin{aligned}\mathbf{R}^*(\mathbf{F}_z) &= \mathbf{R}^*\left(\mathbf{F}_z^0 + \left(\frac{Q_x}{m}\mathbf{e}_1^{\mathrm{T}} + \frac{Q_y}{m}\mathbf{e}_2^{\mathrm{T}}\right)(\mathcal{F}^* - \mathbf{z})\right)\\ &\approx \mathbf{R}^*\left(\mathbf{F}_z^0 + \left(\frac{Q_x}{m}\mathbf{e}_1^{\mathrm{T}} + \frac{Q_y}{m}\mathbf{e}_2^{\mathrm{T}}\right)\mathcal{F}^*\right)\mathbf{R}(\mathcal{F}^*).\end{aligned} \tag{31}$$

Note that, for the cases where non-feasible forces are requested, the variable $\mathbf{z}$ may not comply with the assumption of small allocation errors. Notwithstanding, to handle such cases, we may saturate the calculation of the vertical forces used in the previous relation, thus avoiding negative or excessive vertical loads that appear when dealing with unfeasible forces. Albeit this approach will introduce errors, the resulting weight matrix is still in line with our original goal of assigning higher penalisation to the tyres with lower vertical loads. With this approximation, the dependence on $\mathbf{F}_z$ can be dropped in the cost function, giving $L \approx \|\mathbf{R}(\mathcal{F}^*)\mathbf{F}_{xy}\|^2$; the final control allocation then follows from joining Equations (29)–(31), i.e.

$$\min_{\mathbf{z},\mathbf{F}_{xy},\mathbf{F}_z} \quad \|\mathbf{R}(\mathcal{F}^*)\mathbf{F}_{xy}\|^2 + \|\mathbf{Q}\mathbf{z}\|^2 \quad \text{s.t. (29b)–(29f)}$$

which makes use of $p = 2$ for the norm calculation. Note that $\mathcal{F}^*$ is a parameter of the control allocator; thus, at each update of the control variable, the weight matrix $\mathbf{R}(\mathcal{F}^*)$ is constant, and the cost function quadratic. The main difficulty for the numerical solution of the above problem lies in the second-order cone constraints (29c), which although being convex are not in a suitable format to be handled by real-time QP solvers, like CVXGEN.[30] In the next sub-section, we will discuss two practical algorithms to transform the allocation problem into a QP.

5.4. *Algorithm 1: fix the tyre force angles and then optimise*

The first proposed algorithm is inspired by the CGI method, a widely used allocation strategy in aeronautical applications.[9,10] Our idea builds on the following reasoning: (i) first, we determine a suitable direction for the F_{xi} and F_{yi} forces of each tyre; (ii) then, such direction being kept fixed, the force magnitude is computed so as to fulfil the problem constraints. As will be shown shortly, by fixing the force angles, the second-order cone constraints associated with the friction circle can be transformed into linear inequalities, which are easier to treat numerically.

The algorithm is implemented as follows.

Step 1: First assume that power, torque and friction constraints are not active, and that $\mathcal{F}^*$ is feasible, so $\mathbf{z} = 0$. In these conditions, the control allocation problem (32) can be recast as a minimum-norm problem, subject to equality constraints of the form

$$\min_{\mathbf{F}_{xy}} \quad \|\mathbf{R}(\mathcal{F}^*)\mathbf{F}_{xy}\|^2, \quad \text{s.t.} \quad \mathcal{F}^* = \mathbf{B}\mathbf{F}_{xy}. \tag{32}$$

By constructing the Lagrangian function for the above problem, $\mathcal{L}(\mathbf{F}_{xy}, \lambda) = \|\mathbf{R}(\mathcal{F}^*)\mathbf{F}_{xy}\|^2 + \lambda(\mathbf{B}\mathbf{F}_{xy} - \mathcal{F}^*)$ and applying the first-order optimality conditions ($\partial\mathcal{L}/\partial\mathbf{F}_{xy} = 0, \partial\mathcal{L}/\partial\lambda = 0$), the following analytical solution can be established:

$$\mathbf{F}_{xy}^0 = (\mathbf{R}^{\mathrm{T}}\mathbf{R})^{-1}\mathbf{B}^{\mathrm{T}}(\mathbf{B}(\mathbf{R}^{\mathrm{T}}\mathbf{R})^{-1}\mathbf{B}^{\mathrm{T}})^{-1}\mathcal{F}^*, \tag{33}$$

which is known in the control allocation literature as the weighted pseudo-inverse solution. To simplify the notation, the dependence of $\mathcal{F}^*$ in the weight matrix $\mathbf{R}$ has been omitted.

Step 2: It is obvious that the assumptions made in step 1 do not always hold, and, in practice, the vehicle may have to operate close to the boundaries of the friction/power/torque limits. Consequently, the solution (33) may violate some of the constraints in the problem, and it becomes necessary to rearrange the allocation solution to comply with the constraints. To see how this issue can be handled, it is helpful to express the tyre forces in polar coordinates

$$\mathbf{F}_{xy,i} = \begin{bmatrix} F_{xi} \\ F_{yi} \end{bmatrix} = \rho_i \begin{bmatrix} \cos(\theta_i) \\ \sin(\theta_i) \end{bmatrix}, \quad i \in \mathfrak{T}, \tag{34}$$

where ρ_i is the force magnitude of the tyre $i \in \mathfrak{T}$ and θ_i its angle. Applying the polar representation to all tyre forces $\mathbf{F}_{xy}$, one gets

$$\mathbf{F}_{xy} = \underbrace{\begin{bmatrix} \cos(\theta_{1l}) & 0 & 0 & 0 \\ \sin(\theta_{1l}) & 0 & 0 & 0 \\ 0 & \cos(\theta_{1r}) & 0 & 0 \\ 0 & \sin(\theta_{1r}) & 0 & 0 \\ 0 & 0 & \cos(\theta_{2l}) & 0 \\ 0 & 0 & \sin(\theta_{2l}) & 0 \\ 0 & 0 & 0 & \cos(\theta_{2r}) \\ 0 & 0 & 0 & \sin(\theta_{2r}) \end{bmatrix}}_{\mathbf{H}^*(\theta)} \underbrace{\begin{bmatrix} \rho_{1l} \\ \rho_{1r} \\ \rho_{2l} \\ \rho_{2r} \end{bmatrix}}_{\rho} = \mathbf{H}^*(\theta)\rho, \tag{35}$$

where $\theta = [\theta_{1l} \;\; \theta_{1r} \;\; \theta_{2l} \;\; \theta_{2r}]$ and $\rho \in \mathbb{R}_+^4$. Now, note that, if the angles of the tyre forces θ are fixed, then there is a linear relation between the force magnitude ρ and the $\mathbf{F}_{xy}$. More importantly, the second-order cone constraints associated with the friction limits $\|[F_{xi} \;\; F_{yi}]^{\mathrm{T}}\|_2 \leq \mu_{\max} F_{zi}$ become simple linear inequalities, i.e. $\rho_i \leq \mu_{\max} F_{zi}$. Thus, our approach assumes fixed tyre force angles,

$$\mathbf{H} = \mathbf{H}^*(\theta^0), \tag{36}$$

where θ^0 are the angles obtained from the weighted pseudo-inverse (33). The force magnitude ρ is then redistributed to comply with the friction/power/torque constraints. This redistribution is obtained by inserting Equation (32) in Equation (35) and solving the following problem:

$$\min_{\mathbf{z},\rho,\mathbf{F}_z} \quad \|\mathbf{R}\mathbf{H}\rho\|^2 + \|\mathbf{Q}\mathbf{z}\|^2, \tag{37a}$$

$$\mathcal{F}^* = \mathbf{B}\mathbf{H}\rho + \mathbf{z}, \tag{37b}$$

$$\mathbf{0} \leq \rho \leq \mu_{\max}\mathbf{F}_z, \quad \mathbf{F}_z > 0, \tag{37c}$$

$$\mathbf{F}_z = \mathbf{F}_z^0 + \left(\frac{\varrho_x}{m}\mathbf{e}_1^{\mathrm{T}} + \frac{\varrho_y}{m}\mathbf{e}_2^{\mathrm{T}}\right)\mathbf{B}\mathbf{H}\rho, \tag{37d}$$

$$[1 \;\; 0]\mathbf{E}_i\mathbf{H}\rho \leq \min\left(\frac{\bar{T}}{r_i}, \frac{\bar{P}}{v_x}\right) \quad \forall i \in \mathfrak{T}. \tag{37e}$$

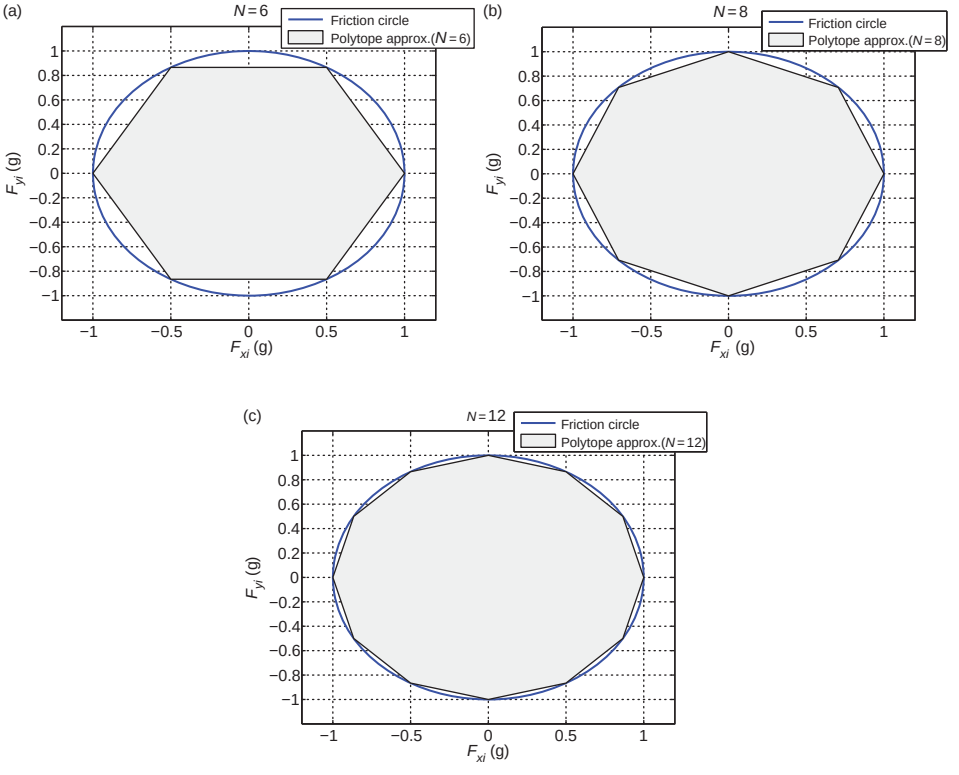

Figure 3. Linear approximation of the friction circle constraints.

It is worth pointing out that all the constraints in the above problem are linear, and the cost function is quadratic[1]; so, we are now in conditions to handle the allocation problem with fast QP solvers. The final allocation solution is then obtained by $\mathbf{F}_{xy} = \mathbf{H}\rho$.

In what follows, the above algorithm will be referred to as PINV + QP.

5.5. *Algorithm 2: linear approximation of the friction circle*

The second algorithm that is proposed to transform Equation (32) into a QP is based on the linearisation of the friction circle constraint. In particular, the main idea is to approximate the circle constraint

$$\left\| \begin{bmatrix} F_{xi} \\ F_{yi} \end{bmatrix} \right\|_2 \leq \mu_{\max} F_{zi}, \quad i \in \mathfrak{T}, \tag{38}$$

by a polytope, characterised by N half-spaces. Namely,

$$\mathbf{C} \begin{bmatrix} F_{xi} \\ F_{yi} \end{bmatrix} \leq \mathbf{D}\mu_{\max} F_{zi}, \quad i \in \mathfrak{T}, \tag{39}$$

where $\mathbf{C} \in \mathbb{R}^{N\times 2}$, $\mathbf{D} \in \mathbb{R}^{N}$ are matrices that characterise the half-spaces (see [21] for the detailed derivation of the matrix expressions). From a qualitative perspective, one may see that, as we increase the number of half-spaces N, the friction circle constraint can be approximated with increasing accuracy (see, e.g. Figure 3 for $N = 12$). However, for the real-time implementation of the allocator, N cannot be too large, as the total number of linear inequalities associated with the friction constraints, taking into account all the tyres, is $4N$. Hence,

in practice, one may need to find a trade-off value for N, capable of providing a reasonable accuracy in the friction circle approximation, but, at the same time, without compromising too much the computational time of the numerical solver (which may be affected by the number of constraints).

Based on the approximation (39), the allocation problem can be posed as

$$\min_{\mathbf{z},\mathbf{F}_{xy},\mathbf{F}_z} \quad \|\mathbf{R}\mathbf{F}_{xy}\|^2 + \|\mathbf{Q}\mathbf{z}\|^2, \tag{40a}$$

$$\mathcal{F}^* = \mathbf{B}\mathbf{F}_{xy} + \mathbf{z}, \tag{40b}$$

$$\mathbf{C}\mathbf{E}_i\mathbf{F}_{xy} \leq \mathbf{D}\mu_{\max}F_{zi}, \quad i \in \mathfrak{T}, \tag{40c}$$

$$\mathbf{F}_z = \mathbf{F}_z^0 + \left(\frac{\varrho_x}{m}\mathbf{e}_1^{\mathrm{T}} + \frac{\varrho_y}{m}\mathbf{e}_2^{\mathrm{T}}\right)\mathbf{B}\mathbf{F}_{xy}, \tag{40d}$$

$$\mathbf{F}_z > 0, \tag{40e}$$

$$[1 \;\; 0]\mathbf{E}_i\mathbf{F}_{xy} \leq \min\left(\frac{\bar{T}}{r_i}, \frac{\bar{P}}{v_x}\right) \quad \forall i \in \mathfrak{T}. \tag{40f}$$

Since all constraints are linear, and the cost function is quadratic,[2] the above problem can be tackled by QP solvers. In comparison with Algorithm 1, the linear approximation requires a larger number of inequalities and optimisation variables, which has an important impact on the computational time. However, the linear approximation has more freedom in selecting the tyre force orientation (recall that in Algorithm 1 the orientation is fixed by the weighted pseudo-inverse), which may be beneficial in situations where non-feasible forces are requested. These properties will be further investigated in the next section, where a detailed comparison between the two algorithms is provided.

It is worth pointing out that, in the context of the control allocation of forces, the linear approximation of the friction circle was an idea initially developed by Jonasson and Andreasson [6]. However, this previous work did not take into account the important influence of the longitudinal and lateral acceleration in the friction circle radius, i.e. Equation (40d), as well as additional power and torque constraints introduced by the IWMs, which are both addressed in this work. Furthermore, we will also investigate how the algorithm performs for different values of N, which is important for its real-time implementation.

In the remainder of this work, the allocator (40) will be named as QP(N), where N refers to the number of linear inequalities employed in the approximations.

5.6. *Comparison of the allocation algorithms*

To investigate the performance of the two allocation algorithms described above, a series of simulation tests is presented. The goal is to evaluate the allocation results during the path following of the Norising track (2.2 km long). The reference force $\mathcal{F}^*$ and the vehicle speed profile $\mathbf{v}$ were generated *via* the FF controller described in Section 4, without activating the FB speed loops. As our concern is now merely focused on the allocation problem, this idealised setting (i.e. the assumption of a perfect vehicle model, without disturbances) constitutes a pragmatic way of gaining insight on the merits and drawbacks of the allocation algorithms. As for numerical solver to handle the QP numerical problems, CVXGEN was used, which is a code-generator tool for embedded linear programming and QP optimisation (see [31] for additional details). We also reduced the number of decision variables in both optimisation problems by eliminating the equality constraints associated with the $\mathbf{z}$ and $\mathbf{F}_z$ variables

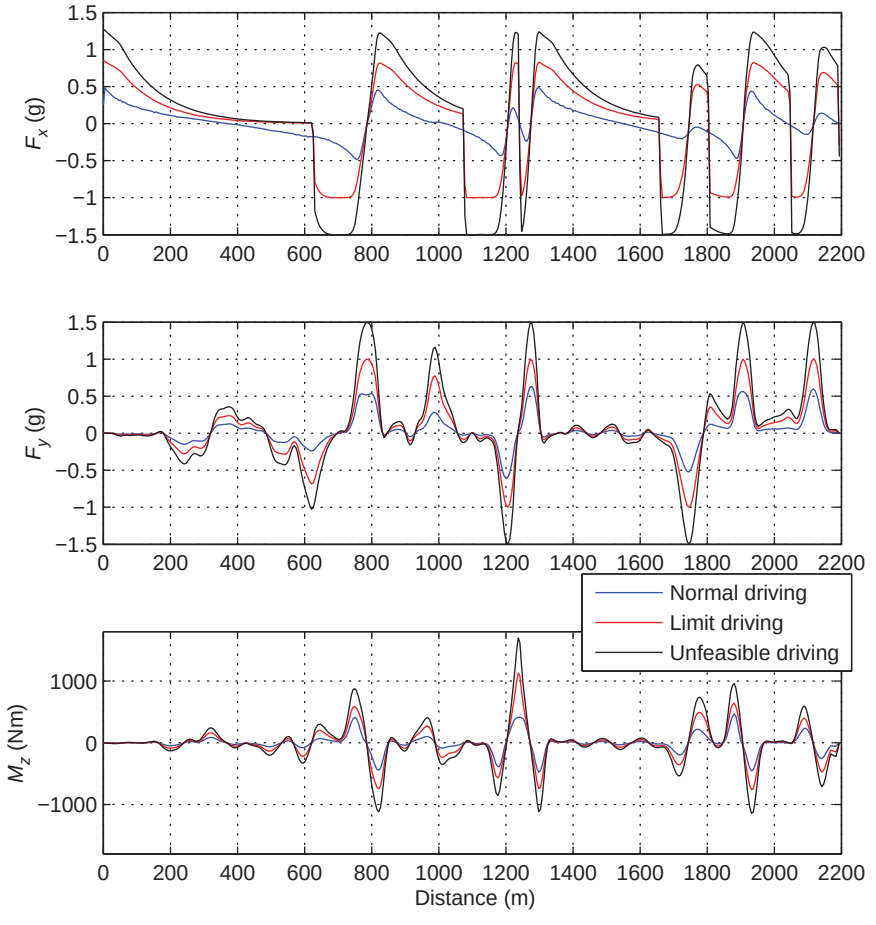

Figure 4. Reference values of $\mathcal{F}^*$ employed in the evaluation of the control allocation algorithms.

(e.g. Equation (40b) was dropped, and the term $\|\mathbf{Qz}\|^2$ replaced by $\|\mathbf{Q}(\mathbf{BF}_{xy} - \mathcal{F}^*)\|^2$). For the performance evaluation of the allocation algorithms, three test cases were considered (Figure 4): (i) normal driving; (ii) limit driving and (iii) unfeasible driving. The normal driving scenario corresponds to the situation where the vehicle is driven around the track with moderate levels of acceleration (lower than $0.5g$). The second case, limit driving, is related to the minimum-time manoeuvring approach, where the vehicle operates very close to the friction and power boundaries. The aim of this test is to assess if the control allocator is able to reach the maximum operation envelope of the vehicle (see [32] and [21] for additional details on the CoG force computation for the minimum-time manoeuvring). In the last scenario, the allocator is asked to produce unfeasible forces, beyond the friction adhesion limits, which is the most challenging task. In this case, the reference force was obtained by rescaling, with a factor of 1.5, the minimum-time solution, i.e. $\mathcal{F}^* = 1.5\mathcal{F}_{\text{min-time}}$.

For each one of these test cases, three allocation strategies will be compared: (i) PINV + QP, (ii) Q ($N = 6$) and (iii) Q ($N = 12$). The latter two were included with the aim of investigating how the parameter N affects the QP performance. Further, to keep the comparison fair, all three algorithms share the same weight matrices.

Figure 5 depicts the mean and maximum allocation errors of the algorithms along the test cases under study. These results show that, for normal driving scenarios, each allocator yields

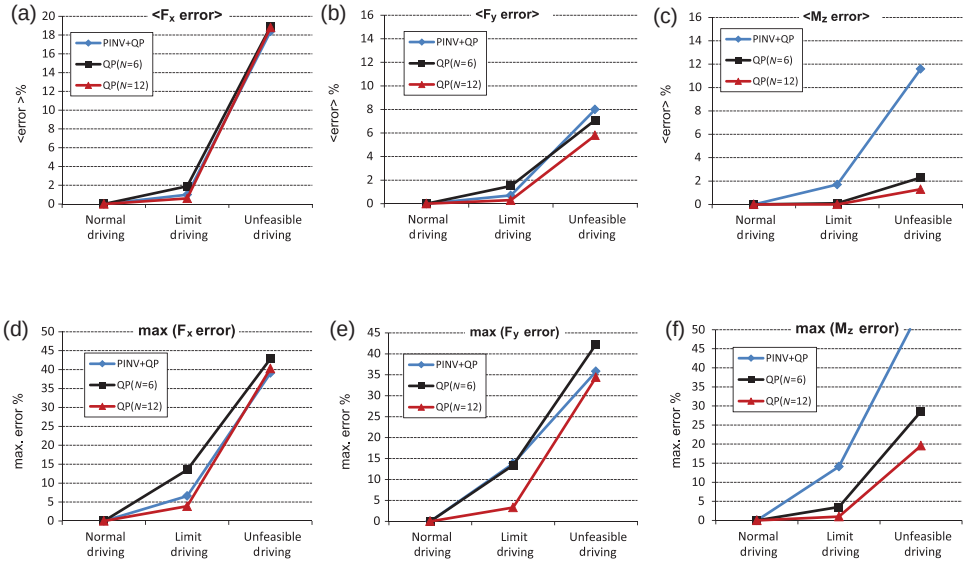

Figure 5. Evaluation of the force errors produced by the allocation algorithms. (a) Mean errors in F_x; (b) mean errors in F_y; (c) mean errors in M_z; (d) max. errors in F_x; (e) max. errors in F_y and (f) max. errors in M_z.

very satisfactory performance, with zero errors. In limit driving conditions, one can find that the average performance of all the allocators is also acceptable, with average errors smaller than 2%. However, the maximum allocation errors for the PINV + QP and QP ($N = 6$) are much higher than those of the QP ($N = 12$); for example, the peak error in the generation of F_y is 14% for both QP ($N = 6$) and PINV + QP, while the QP ($N = 12$) shows only 4%. These results suggests that the full potential of the vehicle may not be reached with the pseudo-inverse allocation and the QP ($N = 6$) strategies; the QP ($N = 12$) method will also be unable to reach the maximum operation envelope, but will be very close. Finally, during the unfeasible driving conditions, the performance of all the allocation algorithms suffers a significant degradation, which was expected given the non-feasible requests. Nonetheless, it can be observed that the QP ($N = 12$) allocation strategy copes better with the infeasibility than the other methods, particularly in the tracking of F_y and M_z. On average, the QP ($N = 12$) features tracking errors of 6% in F_y and 1.8% in M_z, which compares to 8% and 11.8% generated by the PINV + QP, and 7% and 2.1% for the QP ($N = 6$).

From these results, it is clear that the QP ($N = 12$) is the allocation strategy with better performance. The only drawback of this strategy is related to the increase of the computational time; while the difference to the QP ($N = 6$) is not significant (on average, QP ($N = 12$) requires a 30% of extra computational time), the QP ($N = 12$) is 2–2.5 times slower than the pseudo-inverse, as shown in Figure 6. However, the total computational time of the QP ($N = 12$) is, on average, less than 1 ms, which is still acceptable for real-time implementation in a vehicle, where the update rates of the motion controllers are normally of approximately 100 Hz (10 ms).

In view of this analysis, QP ($N = 12$) will be used in the remainder of this article.

5.7. *Tyre force inversion*

After determining the desired x and y forces of each tyre, it is necessary to calculate the corresponding torque T_i and steer angle δ_i, capable of delivering the requested forces. As explained

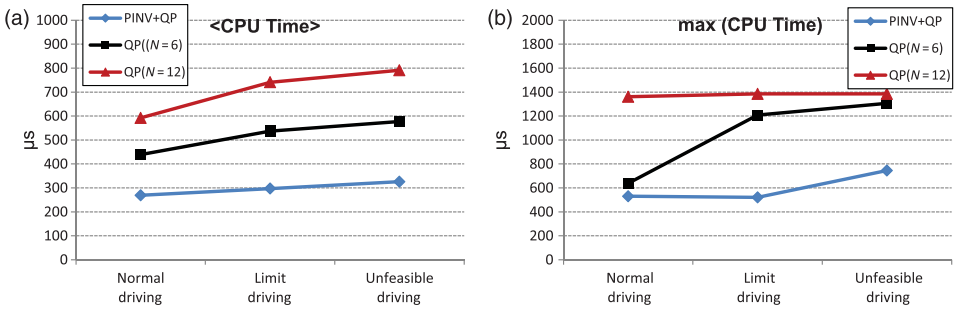

Figure 6. Computational time for the control allocation algorithms. (a) Mean CPU time and (b) max. CPU time.

in [21], this transformation can be performed using the tyre inverse model. However, since, in practice, the tyre model is subject to uncertainty, the tyre inversion will not be *perfect* and, as a result, allocation errors will emerge. In any case, such approximation errors can be embedded in the disturbance term ($\mathcal{D}$) and mitigated by the robust FB loops discussed in the previous section.

6. Simulation results

To evaluate the performance of the proposed control scheme, several tests were carried out with the help of a high-fidelity simulator, the CarSim environment.[33] Since CarSim contemplates dynamics that were neglected at design time, e.g. nonlinear suspension dynamics, compliance effects, roll and pitch motions, etc., this simulation setting enables us to evaluate the robustness of the closed-loop system. The vehicle used in the simulations is based on a B-Class sports car, available in the default library of the CarSim, with the parameters listed in Appendix 2.

6.1. *Double lane change – high μ*

The well-known double lane change (DLC), with normal dry adhesion conditions ($\mu_{\max} = 1$), is the first manoeuvre employed to evaluate the performance of the proposed motion controller. The speed set points $\mathbf{v}_r$ for the vehicle were generated so as to negotiate the DLC at constant longitudinal speed, while keeping the friction force of the tyre (relatively) close to the limits of adhesion. Further, given the high degree of manoeuvrability offered by the 4WS architecture, there are many possibilities to combine the linear and rotational velocity of the vehicle along the DLC. Here we will focus on two particular instances:

- Zero side slip: the vehicle relies only on the yaw rate to change the direction along the trajectory, while keeping the side slip to zero, i.e. $v_{y,r} = 0$.
- Zero yaw rate: only lateral displacement is imposed, without yawing, i.e. $\dot{\psi}_r = 0$.

It is also interesting to investigate the benefits provided by the speed FB loop that is incorporated in the motion controller. To this aim, the DLC was negotiated with and without the speed FB activated. In the latter case, only the FF action is employed.

Analysing the results depicted in Figure 7, one can verify that the FF control action is unable to keep the vehicle within the DLC cones. The reason for this performance degradation is related to the inability of the FF control action alone to counteract disturbances and unmodelled dynamics (and also to the errors in the force allocation process), which

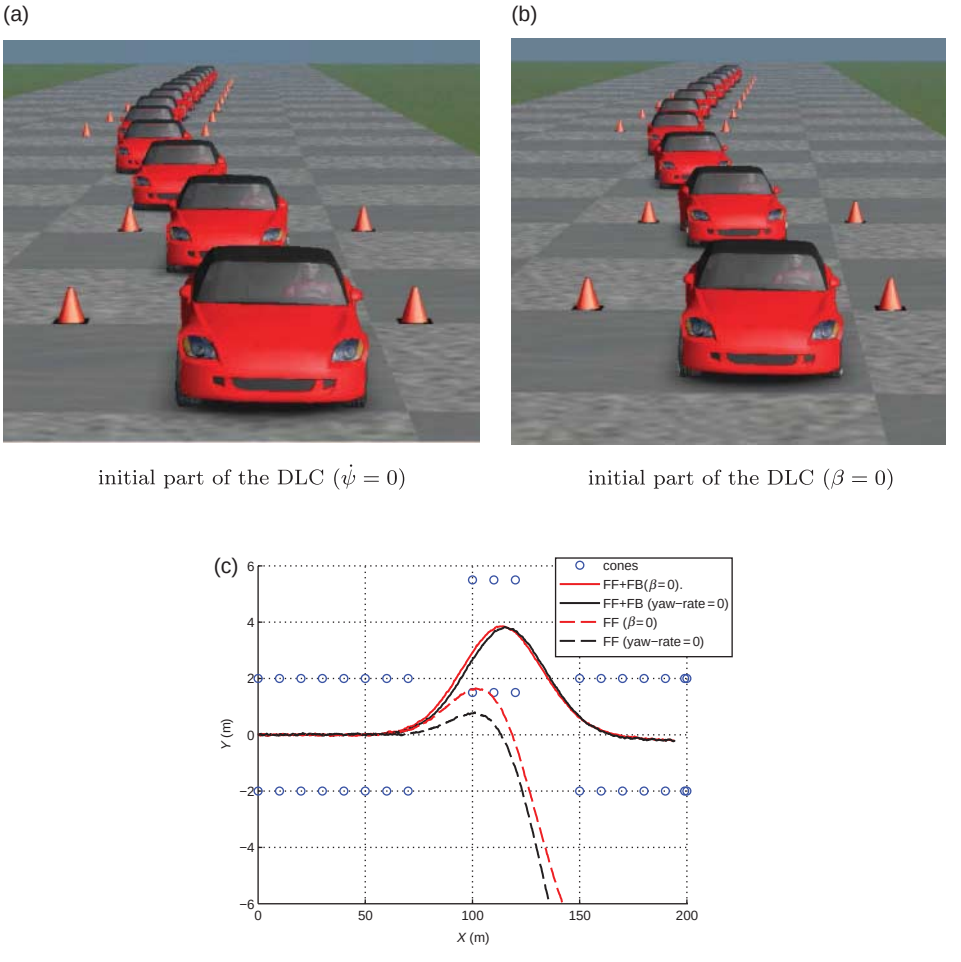

Figure 7. Evolution of the vehicle position when negotiating a DLC with high μ. (a) Initial part of the DLC ($\dot{\psi} = 0$) and (b) initial part of the DLC ($\beta = 0$).

introduce significant discrepancies between the desired motion demand ($\mathbf{v}_r$) and the real vehicle response (Figures 8(a) and 9(a)). On the other hand, by activating the robust FB action, the model mismatches can be attenuated, and the desired vehicle speed $\mathbf{v}_r$ is tracked with good accuracy. To better illustrate this issue, let us look more closely at the yaw dynamics depicted in Figure 8(a); during this test, the controller aims to keep the yaw rate of the car at 0 deg/s, and, as a result, the FF controller is requesting zero yaw moment. However, the simulation results reveal that this control action is insufficient to maintain $\dot{\psi}$ at zero, leading to large tracking errors. Instead, the FF + FB action is able to keep small yaw-rate tracking errors thanks to a significant yaw-moment request.

The two speed references along the DLC manoeuvre also reveal differences in the steering allocation results (Figures 8(b) and 9(b)). For first case – zero yaw-rate approach – the front and rear steering are applied in the same direction and also have approximately the same value. Since the vehicle orientation is intended to be kept constant during the zero yaw-rate approach, this steering policy is reasonable. As for the zero side-slip approach, one may see that the front and rear steer have the same direction, but now the rear steer takes much smaller values. From an engineering perspective, these steering allocation results are explained by

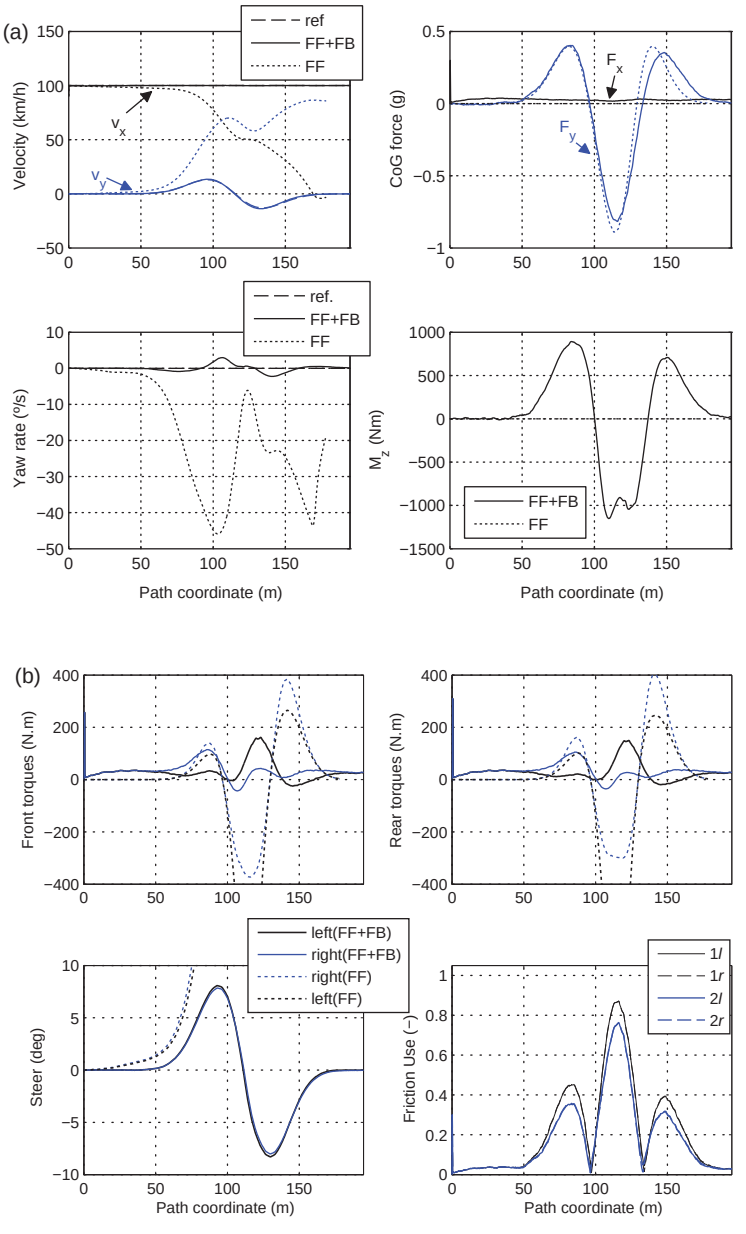

Figure 8. Simulation results when negotiating a DLC (high μ), with a zero yaw-rate policy. (a) CoG speeds and forces/moments and (b) torque and steer allocation; friction usage of the tyres.

the need to generate relatively large yaw moments in the zero side-slip approach. It is also worth mentioning that the torque allocation between left/right wheels contributes with some yaw-moment correction.

6.2. *DLC – low μ*

The goal of the second test is to evaluate the robustness of the motion controller to modelling errors in the estimation of the tyre–road friction coefficient. To do this, the DLC is

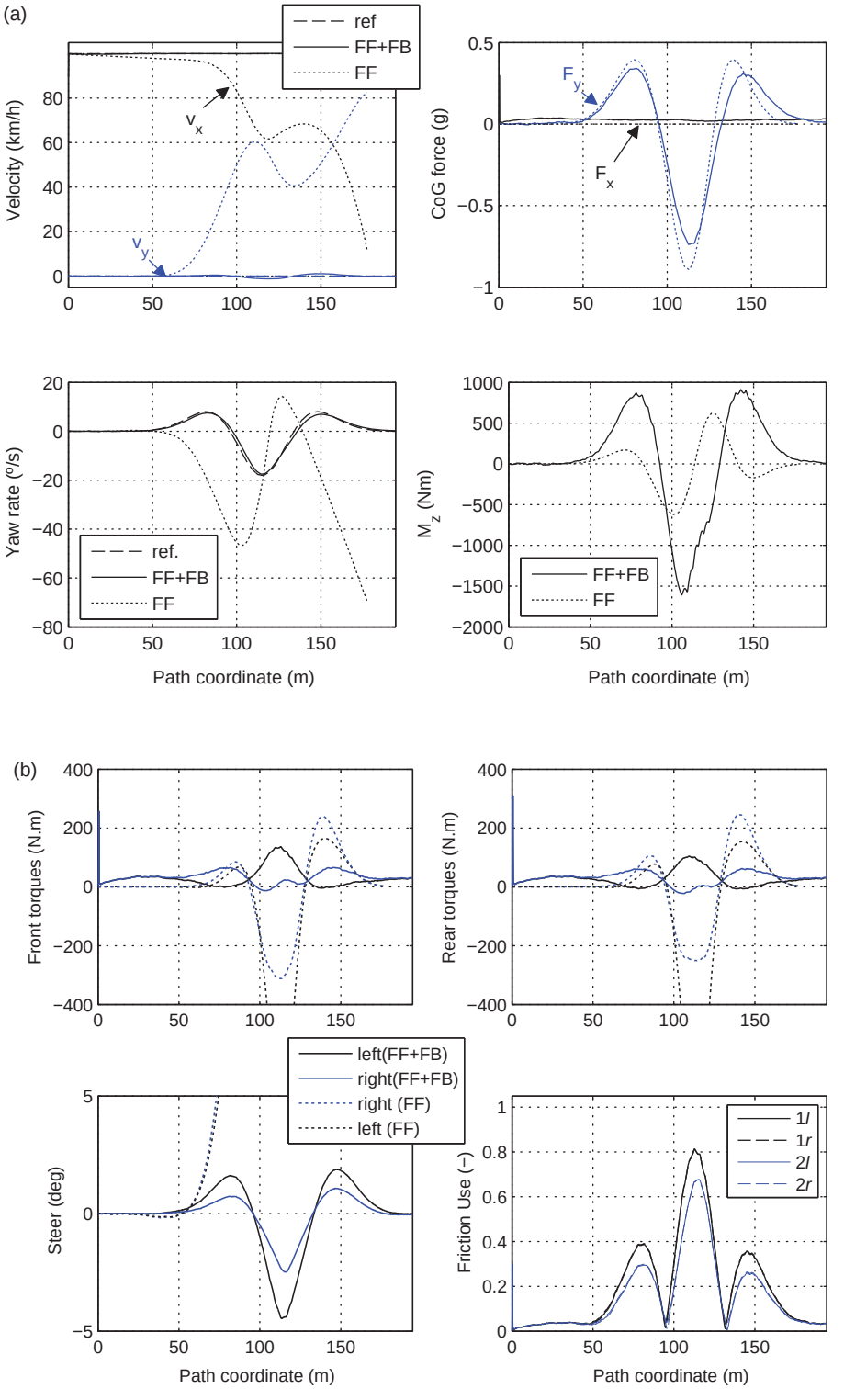

Figure 9. Simulation results when negotiating a DLC (high μ), with a zero side-slip policy. (a) CoG speeds and forces/moments and (b) torque and steer allocation; friction usage of the tyres.

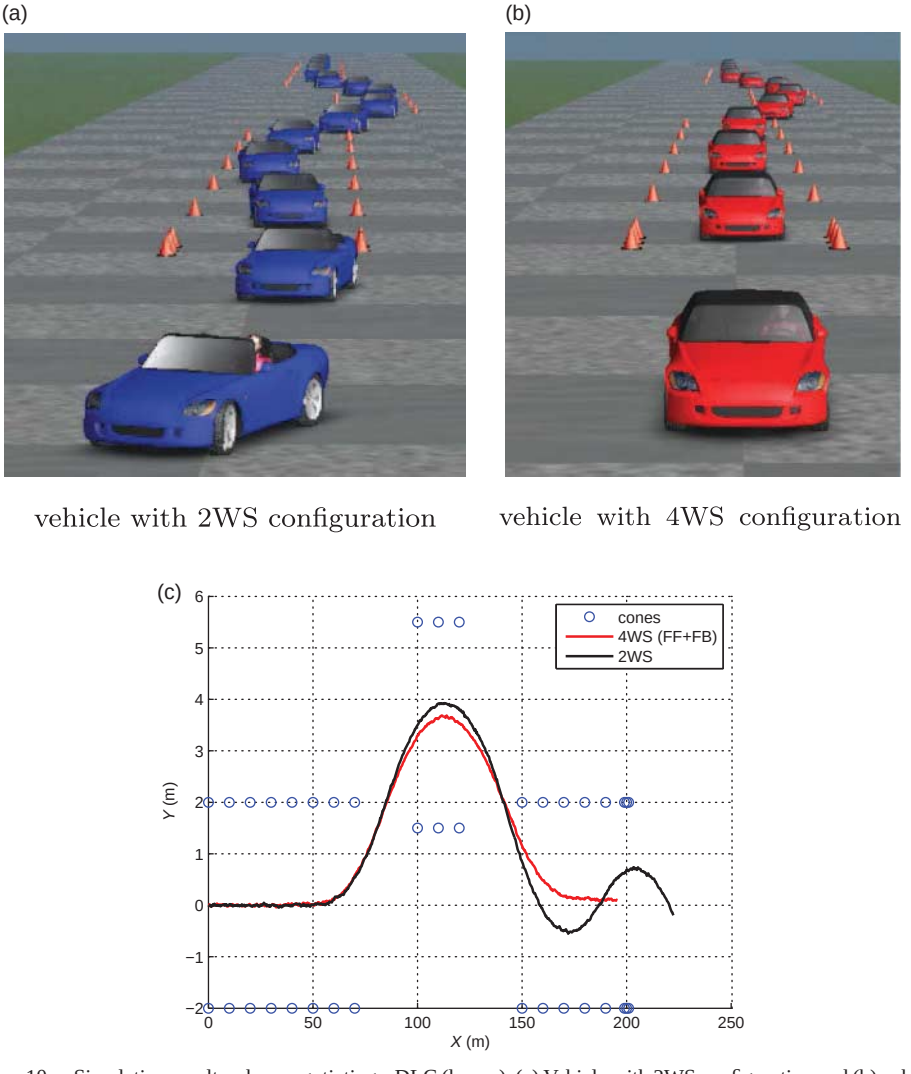

Figure 10. Simulation results when negotiating a DLC (low μ). (a) Vehicle with 2WS configuration and (b) vehicle with 4WS configuration.

negotiated on a low grip surface ($\mu_{\max} = 0.35$), while the motion controller is configured under the assumption of a high tyre–road friction ($\hat{\mu}_{\max} = 1.0$). From the results illustrated in Figures 10 and 11, one can verify that, despite the large friction modelling errors, the proposed motion controller is still capable of negotiating the DLC with safe levels of yaw rate and lateral velocity. Inspecting more closely the allocation results in Figure 11(b), it is worth noting the contribution of the left/right wheel torques to the yaw-moment correction of the vehicle, as well as the (almost) equal distribution of the friction usage between the four tyres (e.g. all four tyres reach the friction saturation approximately at the same time). For comparison purposes, we also performed the same DLC using only front steering; the set point for the front steer was generated through the default path following controller available in CarSim. It can be verified that this 2WS configuration is unable to accomplish the low-mu DLC, leading to a spin at the end of the manoeuvre. These results demonstrate that the proposed motion controller is essential to stabilise the vehicle motion during critical driving conditions.

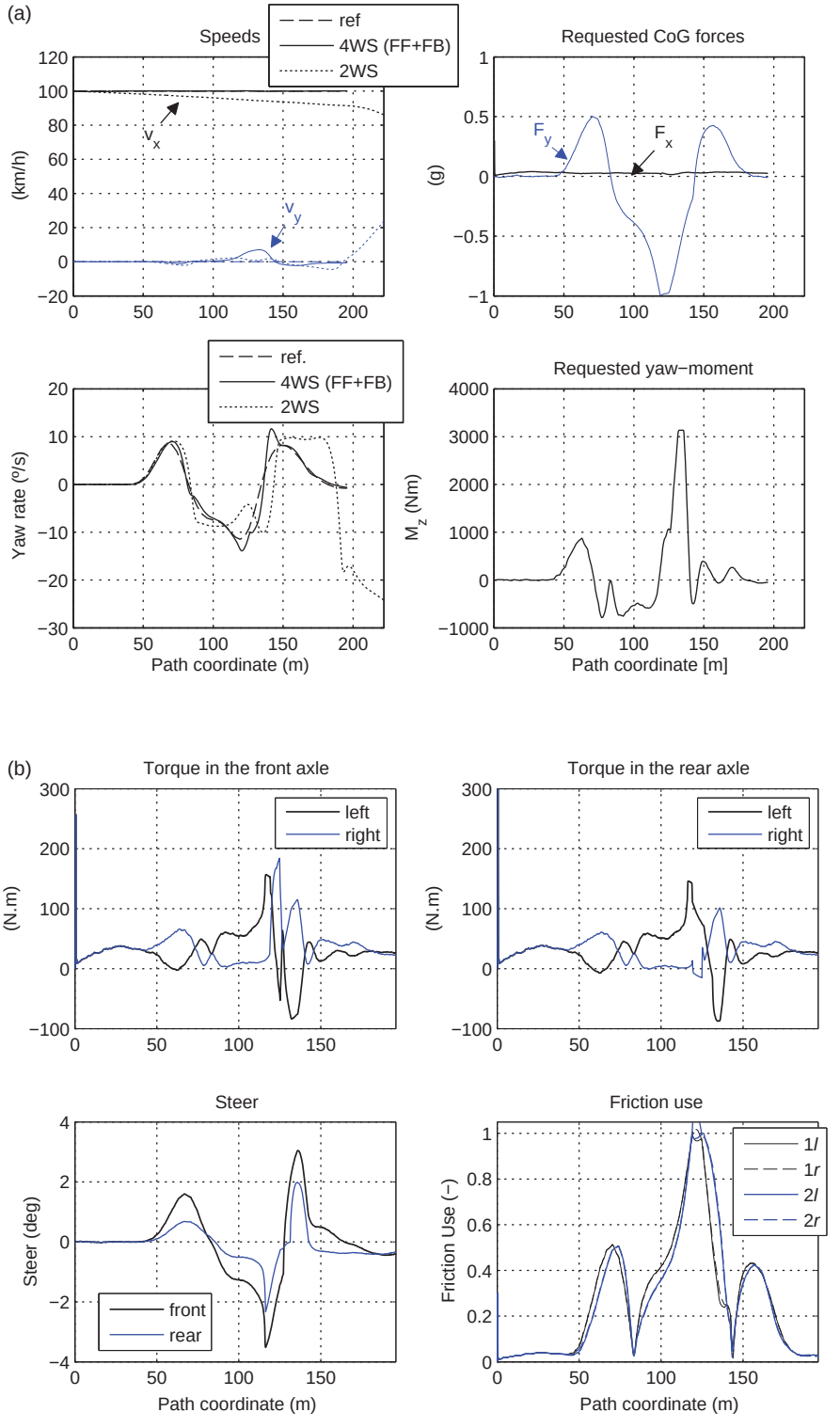

Figure 11. Simulation results when negotiating a DLC (low μ). (a) CoG speeds and forces/moments and (b) torque and steer allocation; friction usage of the tyres.

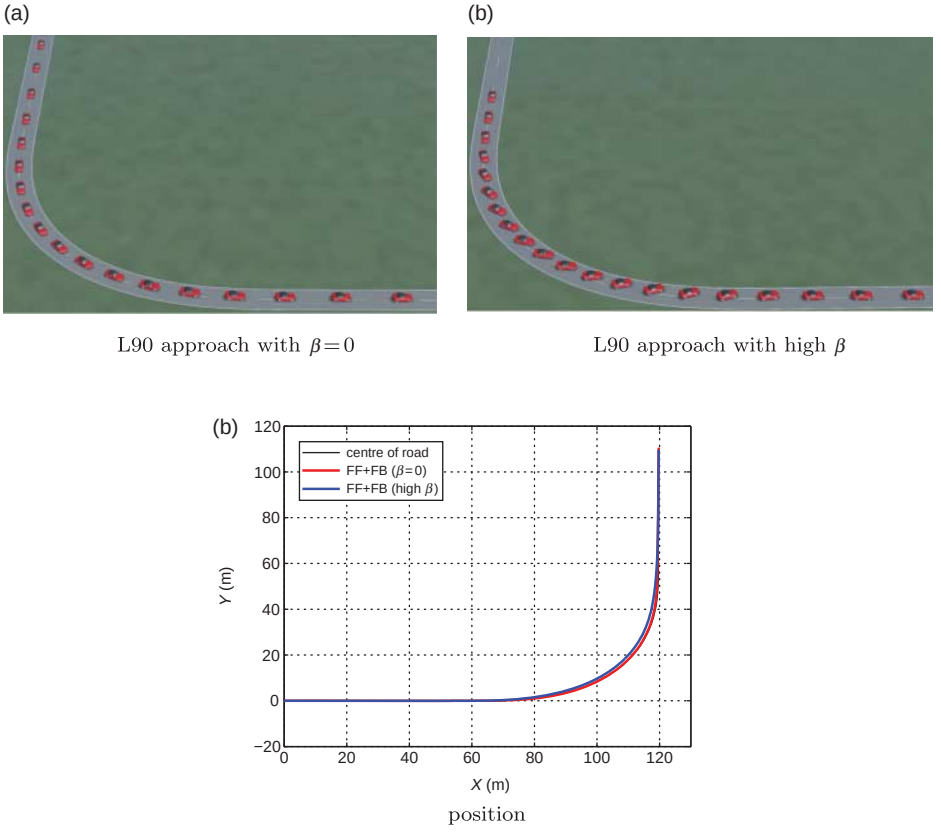

Figure 12. Simulation results when negotiating an L90 corner. (a) L90 approach with $\beta = 0$ and (b) L90 approach with high β.

6.3. *Left* 90° *corner*

The last simulation test analyses the allocation solution when the vehicle is subject to a significant level of combined steering and acceleration/braking. Accordingly, a set of speed profiles $\mathbf{v}_r$ was generated to allow the vehicle to negotiate a left 90° corner (L90) – 40 m radius – with more than $0.5g$ of combined longitudinal and lateral accelerations (see [32] for additional details). Similar to the DLC manoeuvre, two different side-slip policies were evaluated: (i) trajectory following with zero side-slip and (ii) injection of a significant side-slip during the middle of the corner (Figure 12). The results depicted in Figures 13(a) and 14(a) show that, for both policies, the motion controller is able to ensure a good tracking of the reference $\mathbf{v}_r$. Analysing now the torque allocation results with the zero side-slip policy, illustrated in Figure 13(b), a fairly intuitive result is found: during the strong braking phase, $s \in [45, 85]$ m, the controller applies a larger braking torque to the front axle, while the opposite is verified in the accelerating phase, i.e. the rear wheels are given larger torques in the region $s \in [167; 200]$ m. Further, the outer wheels (the right ones in this particular example) are given a larger torque than the inner ones. In view of the load transfer between front–rear axle and left–right wheels that the vehicle experiences when subject to longitudinal and lateral accelerations, these allocation results act to restore the best vehicle stability. In other words, the controller is applying larger torques to the wheels with larger vertical loads. In the *high side-slip manoeuvre*, illustrated in Figure 14, a similar torque split strategy between the

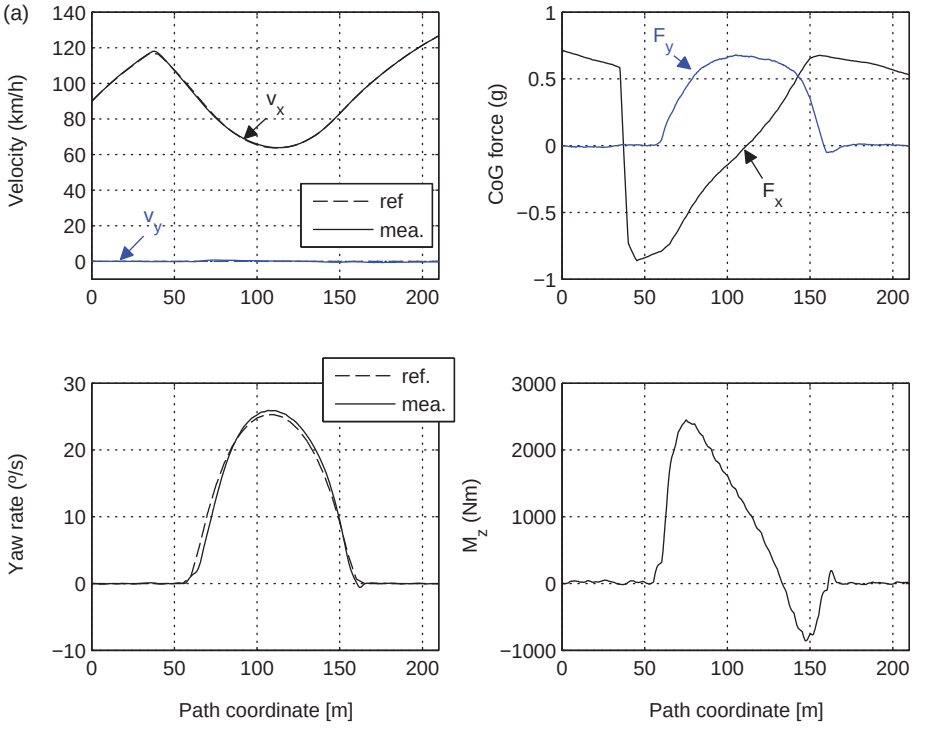

Figure 13. Simulation results when negotiating an L90 corner (zero side-slip). (a) CoG speeds and forces/moments and (b) torque and steer allocation; friction usage of the tyres.

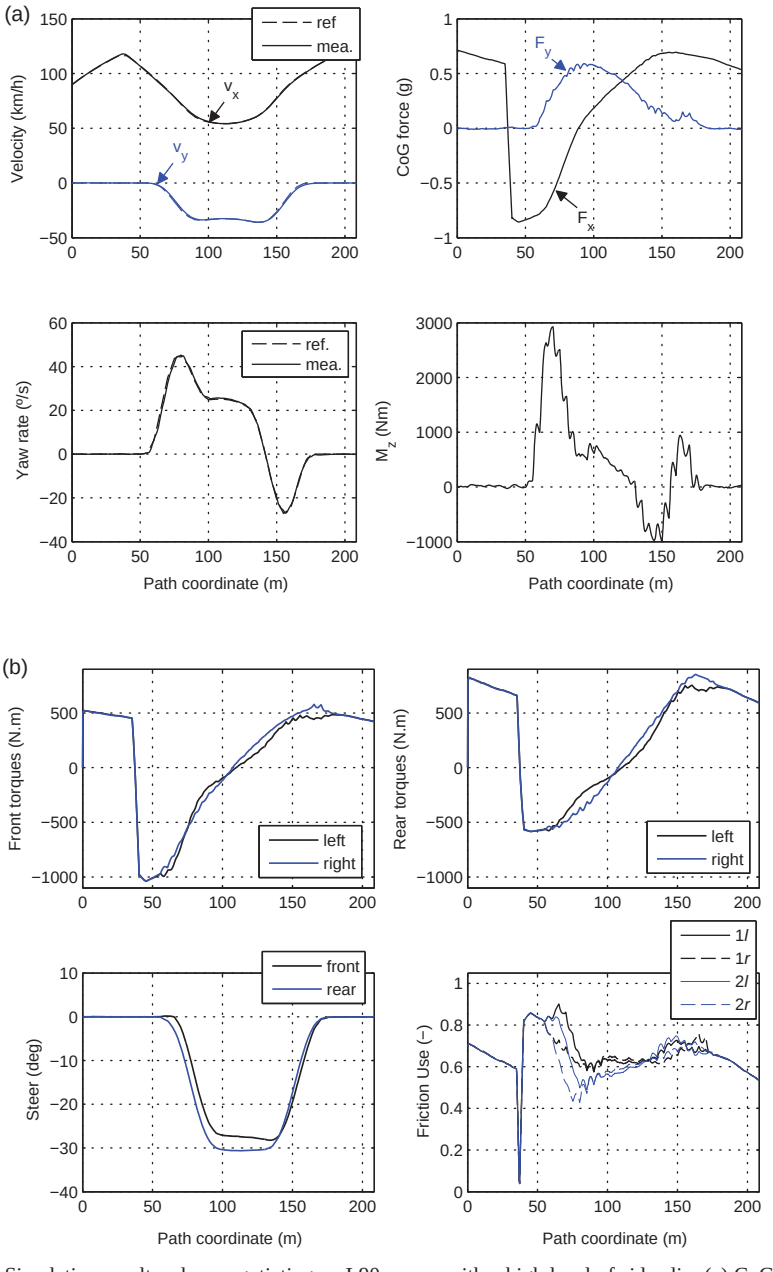

Figure 14. Simulation results when negotiating an L90 corner with a high level of side-slip. (a) CoG speeds and forces/moments and (b) torque and steer allocation; friction usage of the tyres.

wheels can be observed. The major difference with respect to the *zero-slip* approach lies in the steering allocation. More specifically, in the *high side-slip manoeuvre* the front and rear steers, besides being of a significant magnitude, point outside the corner. This behaviour ends up being instrumental to keep the vehicle sliding throughout the turn.

7. Concluding remarks

In this work, a motion control strategy for overactuated EVs has been proposed. Specifically, the full architecture comprising the set point generation, the motion control and the force allocation layer has been designed. The closed-loop stability of the motion control system was formally proved, and a specific attention was devoted to propose force allocation strategies that can meet the real-time requirements of the final application. Simulation results carried out in the full-vehicle CarSim simulation environment demonstrated the effectiveness of the approach, in both normal and extreme driving conditions.

Notes

1. Note that the cost function can be rewritten as $\left\| \begin{bmatrix} \mathbf{RH} & \mathbf{0} \\ \mathbf{0} & \mathbf{Q} \end{bmatrix} \begin{bmatrix} c\rho \\ \mathbf{z} \end{bmatrix} \right\|^2$
2. The cost function can be rewritten as $\left\| \begin{bmatrix} \mathbf{R} & \mathbf{0} \\ \mathbf{0} & \mathbf{Q} \end{bmatrix} \begin{bmatrix} c\mathbf{F}_{xy} \\ \mathbf{z} \end{bmatrix} \right\|^2$.

References

[1] Chen Y, Wang J. Fast and global optimal energy-efficient control allocation with applications to over-actuated electric ground vehicles. IEEE Trans Control Syst Technol. 2012;20(6):2458–2467.
[2] Canale M, Fagiano L, Milanese M, Borodani P. Robust vehicle yaw control using an active differential and imc techniques. Control Eng Pract. 2007;15(8):923–941.
[3] Hancock MJ, Williams RA, Fina E, Best MC. Yaw motion control via active differentials. Trans Inst Meas Control. 2007;29(2):137–157.
[4] Bianchi D, Borri A, Di Benedetto MD, Di Gennaro S. Adaptive integrated vehicle control using active front steering and rear torque vectoring. Int J Veh Auton Syst. 2009;8(2/3/4):85–105.
[5] Juyong K, Jinho Y, Kyongsu Y. Driving control algorithm for maneuverability, lateral stability, and rollover prevention of 4wd electric vehicles with independently driven front and rear wheels. IEEE Trans Veh Technol. 2011;60(7):2987–3001.
[6] Jonasson M, Andreasson J. Exploiting autonomous corner modules to resolve force constraints in the tyre contact patch. Veh Syst Dyn. 2008;46(7):553–573.
[7] Wang JM, Longoria RG. Coordinated and reconfigurable vehicle dynamics control. IEEE Trans Control Syst Technol. 2009;17(3):723–732.
[8] Danwei W, Feng Q. Trajectory planning for a four-wheel-steering vehicle. Proceedings 2001 ICRA. IEEE International Conference on Robotics and Automation, Volume 4; Seoul, Korea; 2001. p. 3320–3325.
[9] Jin JY. Modified pseudoinverse redistribution methods for redundant controls allocation. J Guidance Control Dyn. 2005;28(5):1076–1079.
[10] Virnig JC, Bodden DS. Multivariable control allocation and control law conditioning when control effectors limit. AIAA Guidance, Navigation, and Control Conference and Exhibit, Scottsdale; 1994.
[11] Seshagiri S, Khalil HK. Robust output feedback regulation of minimum-phase nonlinear systems using conditional integrators. Automatica. 2005;41(1):43–54.
[12] Seshagiri S, Khalil HK. Universal integral controllers with anti-reset windup for minimum phase nonlinear systems. Proceedings of the 40th IEEE Conference on Decision and Control; Hyatt Regency Grand Cypress Resort, Orlando, USA; 2001.
[13] de Castro R, Tanelli M, Araujo RE, Savaresi S, Freitas D. Torque allocation in evs with 4 in-wheel motors: a high-performance approach. Proceedings of the 23nd International Symposium on Dynamics of Vehicles on Roads and Tracks (IAVSD13); 2013; Qingdao, China.
[14] Geng C, Mostefai L, Denai M, Hori Y. Direct yaw-moment control of an in-wheel-motored electric vehicle based on body slip angle fuzzy observer. IEEE Trans Ind Electron. 2009;56(5):1411–1419.
[15] Pacejka HB. Tyre and vehicle dynamics. Oxford: Butterworth-Heinemann; 2002.
[16] Kiencke U, Nielsen L. Automotive control systems for engine, driveline, and vehicle. Heidelberg: Springer-Verlag; 2005.
[17] Gillespie TD. Fundamentals of vehicle dynamics. Warrendale (PA): Society of Automotive Engineers, Inc. 1992.
[18] de Castro R, Araujo RE, Tanelli M, Savaresi S, Freitas D. Torque blending and wheel slip control in evs with in-wheel motors. Veh Syst Dyn. 2012;50(supp. 1):71–94.
[19] Kirstin L. Talvala R, Kritayakirana K, Gerdes JC. Pushing the limits: From lanekeeping to autonomous racing. Annu Rev Control. 2011;35(1):137–148.
[20] Khalil H. Nonlinear systems. 3rd ed. Upper Saddle River (NJ): Prentice Hall; 2002.

[21] de Castro R. Motion control and energy management of electric vehicles [PhD thesis]. Porto: Faculdade de Engenharia da Universidade do Porto; 2013.
[22] Bodson M. Evaluation of optimization methods for control allocation. J Guidance Control Dyn. 2002;25(4):703–711.
[23] Fossen TI, Johansen TA, Perez T. A survey of control allocation methods for underwater vehicles. Vienna: I-Tech Education and Publishing; 2009. Chapter 7.
[24] Bayar K, Wang J, Rizzoni G. Development of a vehicle stability control strategy for a hybrid electric vehicle equipped with axle motors. Proc Inst Mech Eng D J Automob Eng. 2012;226(6):795–814.
[25] Plumlee JH, Bevly DM, Hodel AS. Control allocation in ground vehicles. Int J Veh Des. 2006;42(3–4):215–243.
[26] Boyd S, Vandenberghe L. Convex optimization. Cambridge (UK): Cambridge University Press; 2004.
[27] Ono E, Hattori Y, Muragishi Y, Koibuchi K. Vehicle dynamics integrated control for four-wheel-distributed steering and four-wheel-distributed traction/braking systems. Veh Syst Dyn: Int J Veh Mech Mobility. 2006;44(2):139–151.
[28] Weiskircher T, Müller S. Control performance of a road vehicle with four independent single-wheel electric motors and steer-by-wire system. Veh Syst Dyn. 2012;50(supp. 1):53–69.
[29] Jonasson M, Andreasson J, Solyom S, Jacobson B, Trigell AS. Utilization of actuators to improve vehicle stability at the limit: from hydraulic brakes toward electric propulsion. J Dyn Syst Meas Control. 2011;133(5):051003-1–051003-10.
[30] CVX Research, Inc. CVX: Matlab software for disciplined convex programming, version 2.0 beta; 2012.
[31] Mattingley J, Boyd S. Cvxgen: a code generator for embedded convex optimization. Optim Eng. 2012;13(1):1–27.
[32] de Castro R, Tanelli M, Araujo RE, Savaresi SM. Minimum-time path following in highly redundant electric vehicles. Proceedings of the 19th IFAC World Congress; 2014; Cape Town. To appear.
[33] Carsim 8.0 user manual. Mechanical Simulation Corporation; 2009. Available from: http://www.carsim.com/products/carsim/index.php.

Appendix 1. Resistance forces

The main resistance forces that affect the vehicle motion are assumed to be rolling friction and aerodynamic drag. Road grade forces were neglected, since only planar motion is considered. Thus, the resistance force can be expressed as

$$\mathcal{R}(\mathbf{v}) = \begin{bmatrix} \mathcal{R}_x \\ \mathcal{R}_y \\ \mathcal{R}_\psi \end{bmatrix} = \begin{bmatrix} mgf_r \\ 0 \\ 0 \end{bmatrix} + \frac{1}{2}\rho \begin{bmatrix} A_x C_x(\beta)|v_x|v_x \\ A_y C_y(\beta)|v_y|v_y \\ 0 \end{bmatrix}, \tag{A1}$$

where f_r is the rolling resistance coefficient, ρ represents the air density, A_j the vehicle area in the direction $j \in \{x, y\}$ and C_j the drag coefficient, which may be dependent on the vehicle side-slip angle $\beta = \text{atan}(v_x/v_y)$.[17]

Appendix 2. Parameters of the model and controller

See Table A1.

Table A1. Vehicle and controller parameters.

Variable	Symbol	Value
Vehicle mass	m	1100 kg
Yaw inertia	I_z	996 kg m^2
Distance between front axle and COG	l_1	1.2 m
Distance between rear axle and COG	l_2	1.3 m
COG height	h	0.37 m
Track width	c	1.5 m
Rolling resistance	f_r	0.004
Aero. drag coefficient (frontal)	C_x	0.35
Aero. drag coefficient (lateral)	C_y	0.7
Frontal area	A_x	1.6 m
Lateral area	A_y	1.6 m
Air density	ρ	1.206 kg/m^3
Wheel radius	r	0.3 [m]
MTF parameter A	B	7
MTF parameter B	C	1.6
MTF parameter C	D	1
Maximum power/IWM	$\bar{P}$	36 kW
Maximum torque/IWM	$\bar{T}$	777 Nm
Parameters of the speed controller		
$[k_{ax}, k_{ay}, k_{a\psi}]$		[2.9, 4.9, 2.6]
$[k_{\eta x}, k_{\eta y}, k_{\eta\psi}]$		[2.2, 0.7, 3.1]
$[\varepsilon_x, \varepsilon_y, \varepsilon_\psi]$		[1.7, 1.1, 0.14]
Control allocation		
$\mathbf{Q}$		diag([1, 1, 5])

Note: MTF; Magic tyre formula.

Appendix 3. Approximation of torque and power constrains

To make torque and power constraints of the electric motors and friction brakes in Equation (10) manageable in the allocation process, the main idea is to express them as functions of (v_x, F_{xi}), instead that in the original coordinates (ω_i, T_i). To do this, we assume steady conditions for the wheel dynamics (10), which are much faster than the chassis ones that the controller aims at regulating. Thus, one has

$$T_i \approx r_i F_{\mathrm{L}i}, \quad i \in \mathfrak{T}. \tag{A2}$$

Further, the tyre longitudinal slips will be neglected, which allows us to approximate the wheel rotational velocity as $\omega_i \approx v_x/r_i$. Finally, the wheel steering angles δ_i are assumed to be small, enabling us to approximate $\mathbf{W}(\delta_i) \approx \mathbf{I}$, where $\mathbf{I}$ is the identify matrix. Under these assumptions, the power and torque limits (10) can be approximated as

$$\underline{T} \le F_{x,i} r_i \le \bar{T}, \quad F_{x,i} v_x \le \bar{P}, \quad i \in \mathfrak{T}. \tag{A3}$$

Moreover, assuming that $\underline{T}$, provided by the friction brakes, is always capable to overcome the friction limits of the tyre–road adhesion, then the lower inequality in $F_{x,i}$ can be neglected. This allows us to rewrite the previous constraints as

$$F_{x,i} \le \min\left(\frac{\bar{T}}{r_i}, \frac{\bar{P}}{v_x}\right), \quad i \in \mathfrak{T}. \tag{A4}$$

The above set provides a very reasonable approximation of the torque/power constraints in straight-line conditions, its accuracy degrading when the cornering manoeuvres become more aggressive (i.e. when δ_i increases). Nevertheless, since during cornering conditions the longitudinal accelerations are normally low, the above approximated sets proved to yield good performance in the allocation scheme.